

## The organization of the human striatum estimated by intrinsic functional connectivity

Eun Young Choi,<sup>1,2,3</sup> B. T. Thomas Yeo,<sup>2,3,4</sup> and Randy L. Buckner<sup>2,3,5,6</sup>

<sup>1</sup>Program in Neuroscience, Division of Medical Sciences, Harvard University, Cambridge, Massachusetts; <sup>2</sup>Harvard University Department of Psychology, Center for Brain Science, Cambridge, Massachusetts; <sup>3</sup>Athinoula A. Martinos Center for Biomedical Imaging, Department of Radiology, Massachusetts General Hospital, Charlestown, Massachusetts; <sup>4</sup>Neuroscience and Behavioral Disorders Program, Duke-NUS Graduate Medical School, Singapore; <sup>5</sup>Howard Hughes Medical Institute, Cambridge, Massachusetts; and <sup>6</sup>Department of Psychiatry, Massachusetts General Hospital, Boston, Massachusetts

Submitted 30 March 2012; accepted in final form 17 July 2012

**Choi EY, Yeo BT, Buckner RL.** The organization of the human striatum estimated by intrinsic functional connectivity. *J Neurophysiol* 108: 2242–2263, 2012. First published July 25, 2012; doi:10.1152/jn.00270.2012.—The striatum is connected to the cerebral cortex through multiple anatomical loops that process sensory, limbic, and heteromodal information. Tract-tracing studies in the monkey reveal that these corticostriatal connections form stereotyped patterns in the striatum. Here the organization of the striatum was explored in the human with resting-state functional connectivity MRI (fcMRI). Data from 1,000 subjects were registered with nonlinear deformation of the striatum in combination with surface-based alignment of the cerebral cortex. fcMRI maps derived from seed regions placed in the foot and tongue representations of the motor cortex yielded the expected inverted somatotopy in the putamen. fcMRI maps derived from the supplementary motor area were located medially to the primary motor representation, also consistent with anatomical studies. The topography of the complete striatum was estimated and replicated by assigning each voxel in the striatum to its most strongly correlated cortical network in two independent groups of 500 subjects. The results revealed at least five cortical zones in the striatum linked to sensorimotor, premotor, limbic, and two association networks with a topography globally consistent with monkey anatomical studies. The majority of the human striatum was coupled to cortical association networks. Examining these association networks further revealed details that fractionated the five major networks. The resulting estimates of striatal organization provide a reference for exploring how the striatum contributes to processing motor, limbic, and heteromodal information through multiple large-scale corticostriatal circuits.

somatotopy; limbic network; prefrontal cortex; association cortex; fMRI; functional connectivity; default network

ANIMAL STUDIES and human patient cases demonstrate that the basal ganglia are involved in diverse functional domains including movement, cognition, and reward (Alexander et al. 1986; DeLong and Georgopoulos 1981; Haber and Gdowski 2004; MacLean 1972). Providing an anatomical basis for functional diversity, tract-tracing studies show that the basal ganglia are connected to distributed regions of the cerebral cortex through multiple, partially parallel anatomical loops (Alexander et al. 1986, 1990). Each loop includes projections from the cerebral cortex, through the basal ganglia, to the thalamus, and back to the cerebral cortex. Cortical efferents to the striatum (the main input nucleus of the basal ganglia) form distinct patterns depending on their cortical origin. The posterior putamen and the dorsolateral anterior putamen receive projections from motor and motor association cortex,

the central anterior striatum from cognitive regions including prefrontal cortex, and the ventral anterior striatum from regions associated with the limbic system, in particular medial and orbital frontal cortex (Haber et al. 1994; Parent 1990). More complex projection patterns are also observed that do not fit neatly into a tripartite heuristic, including interdigitated projection zones (Sellen and Goldman-Rakic 1985). Nonetheless, corticostriatal projections in the monkey broadly differentiate motor, cognitive, and affective systems, suggesting a basis for functional specialization within the basal ganglia. Characterizing the detailed topography of corticostriatal projections in the human is thus important for understanding basal ganglia function and how motor and neuropsychiatric disorders arise from its dysfunction.

### Organization of the Striatum in the Human

Corticostriatal projections in the human have been explored with noninvasive neuroimaging methods including intrinsic functional connectivity (Barnes et al. 2010; Di Martino et al. 2008; Zhang et al. 2008), diffusion tensor imaging (DTI; Draganski et al. 2008; Leh et al. 2007; Lehéricy et al. 2004), T1-weighted voxel-based morphometry (VBM; Cohen et al. 2008), and meta-analysis of corticostriatal coactivation in task-based functional studies (Postuma and Dagher 2006). Consistent with estimates of striatal organization in the monkey, these studies reveal broad topographic patterns that differentiate motor, cognitive, and affective zones of the striatum. For example, using DTI, Lehéricy et al. (2004) examined white matter tracts arising from seed regions placed within the striatum. The posterior putamen gave rise to fiber tracts that traveled through the corona radiata to the motor and adjacent premotor cortices, the anterior striatum targeted the prefrontal cortex and pre-supplementary motor area (pre-SMA), and the ventral striatum revealed tracts associated with the orbital frontal and temporal cortices. Draganski et al. (2008) mapped the detailed voxel connectivity profiles of each point in the human striatum to 23 regions distributed throughout the ipsilateral cerebral hemisphere. The estimated topography demonstrated the tripartite division. More detailed analysis also revealed a functional gradient within the striatum as suggested by Haber (2003) based on animal tracing studies.

Intrinsic functional connectivity MRI (fcMRI; Biswal et al. 1995) has recently emerged as a complementary tool to map the organization of corticostriatal circuits. The basis and limitations of fcMRI are discussed in our companion papers (Buckner et al. 2011; Yeo et al. 2011) and elsewhere (Buckner 2010; Fornito and Bullmore 2010; Fox and Raichle 2007; Power et al. 2010; Van Dijk et al. 2010). fcMRI detects low-frequency correlations be-

Address for reprint requests and other correspondence: R. L. Buckner, Harvard Univ., 52 Oxford St., Northwest Bldg., 280.06, Cambridge, MA 02138 (e-mail: randy\_buckner@harvard.edu).

tween regions of the brain. The correlations are constrained by polysynaptic anatomical connectivity (although other factors also contribute to functional coupling) such that two regions that are anatomically connected will tend to show stronger functional coupling measured at rest. Thus it is possible to map striatal organization by examining the functional coupling patterns between the striatum and the cerebral cortex.

Di Martino et al. (2008) were among the first to systematically explore striatal organization with fcMRI. By examining the cerebral coupling patterns from six seed regions placed throughout the striatum, they demonstrated clear functional subdivisions. However, the patterns of cortical coupling did not simply involve discrete regions of cortex. Rather, individual striatal regions were coupled to widespread cortical targets. For example, the seed region placed in the right dorsal caudate was functionally correlated with bilateral regions of the dorsolateral prefrontal cortex, anterior cingulate, posterior cingulate, and the inferior parietal lobule (e.g., see their Fig. 3).

In a recent fcMRI exploration of the striatum, Barnes et al. (2010) employed graph analytic techniques. With a procedure conceptually similar to the DTI work of Draganski et al. (2008), the profile of functional connectivity for each striatal voxel was analyzed to identify clusters of voxels with similar cortical connectivity patterns. They found that at least three clusters of striatal voxels could be grouped together on the basis of their similar coupling patterns to distinct, distributed cortical networks (forming modules). Thus the analyses of both Di Martino et al. (2008) and Barnes et al. (2010), while consistent with distinctions between motor, cognitive, and affective systems, also suggest that striatal functional coupling is not localized to discrete portions of a specific lobe or cortical region. Rather, striatal regions are functionally coupled to distributed regions throughout the cerebral cortex.

### Present Study

The present study builds upon these prior studies, using an approach that follows from our recent companion papers (Buckner et al. 2011; Yeo et al. 2011). We previously identified functionally coupled networks across the cerebral cortex (Yeo et al. 2011; see also Power et al. 2011) that provided a basis for mapping the cerebellum (Buckner et al. 2011). Here each striatal voxel was mapped to its most correlated cortical network, thereby comprehensively mapping the striatum in reference to cerebral networks. In this regard, the present strategy differs from prior studies of the striatum that target specific anatomically defined cortical targets (e.g., dorsolateral prefrontal cortex). The goals of this study are 1) to provide reference maps that are a current best estimate of the organization of the human striatum as measured by functional connectivity, 2) to compare human striatal functional connectivity to monkey anatomical connectivity, and 3) to explore whether there are any global patterns that provide insight into cortico-striatal circuit organization in the human.

## METHODS

### Overview

The present study consists of three analyses. First, the feasibility of mapping specific corticostriatal circuits with fcMRI was explored by examining the correlations between the motor cortex and the striatum,

for which there are strong predictions from monkey tract-tracing studies.

Having observed that fcMRI can reveal motor-related topographical properties of the striatum, we next comprehensively mapped the functional connectivity between the striatum and the entire cerebral cortex. This was done by assigning each striatal voxel to its most strongly correlated cortical network in 500 subjects (discovery sample) and replicating the topography in an independent sample of 500 subjects (replication sample). The cortical networks were defined by a clustering method developed in our companion paper (Yeo et al. 2011) that parcellates the cerebral cortex into networks of regions that have similar profiles of corticocortical functional connectivity. After the reliability of the maps was demonstrated, all 1,000 subjects were used to provide a best estimate of the striatal topography based on coarse (7-network) and fine (17-network) parcellations of the cerebral cortex.

In the third analysis, we explored striatal networks in greater detail. We assessed the parcellations, using a quantitative analysis of corticostriatal specificity and qualitative comparisons of how well seed-based cortical fcMRI maps agreed with monkey anatomical studies. We compared the human functional connectivity estimates to monkey anatomical cases located across the motor, association, and limbic networks. We also compared cases within the same association networks. Finally, we examined subdivisions of the association networks in the 17-network parcellation of the striatum in greater detail to explore finer distinctions suggested by the functional connectivity analysis. For all analyses, seed regions were identified in the discovery sample or an outside source such as an fMRI task, and functional connectivity was quantified in the independent replication sample to avoid bias.

### Participants

One thousand paid participants ages 18–35 yr were clinically normal, English-speaking young adults with normal or corrected-to-normal vision. The subjects are the same individuals as reported in Yeo et al. (2011) and Buckner et al. (2011). Subjects were excluded if their slice-based fMRI signal-to-noise ratio (SNR) was low (<100; Van Dijk et al. 2012), artifacts were detected in the MR data, their self-reported health information indicated a history of neurological or psychiatric illness, or they were taking psychoactive medications. The subjects were imaged during eyes-open rest and divided into two samples (each  $n = 500$ ) matched for age and sex: discovery (mean age = 21.3 yr, 42.6% male) and replication (mean age = 21.3 yr, 42.8% male) samples. Participants provided written informed consent in accordance with protocols reviewed and approved by institutional review boards of Harvard University or Partners Healthcare.

### MRI Data Acquisition

All data were collected on matched 3T Tim Trio scanners (Siemens, Erlangen, Germany) with the vendor-supplied 12-channel phased-array head coil. The functional imaging data were acquired with a gradient-echo echo-planar imaging (EPI) sequence sensitive to blood oxygenation level-dependent (BOLD) contrast (Kwong et al. 1992; Ogawa et al. 1992). Whole brain coverage was achieved with 47 3-mm slices aligned to the anterior commissure-posterior commissure (AC-PC) plane with automated alignment (van der Kouwe et al. 2005). Structural data included a high-resolution multiecho T1-weighted magnetization-prepared gradient-echo image (multiecho MP-RAGE; van der Kouwe et al. 2008). Functional imaging parameters were TR = 3,000 ms, TE = 30 ms, flip angle = 85°, 3 × 3 × 3-mm voxels, FOV = 216, and 47 slices. Structural scan (multiecho MP-RAGE) parameters were TR = 2,200 ms, TI = 1,100 ms, TE = 1.54 ms for *image 1* to 7.01 ms for *image 4*, flip angle = 7°, 1.2 × 1.2 × 1.2-mm voxels, and FOV = 230. During the functional scans, subjects were instructed to stay still, stay awake, and

keep their eyes open. Resting-state data acquisition is described in detail in Yeo et al. (2011).

#### *Functional MRI Data Preprocessing*

fMRI data were preprocessed as described in Yeo et al. (2011). Briefly, the first four volumes of each run were discarded, slice acquisition-dependent time shifts were compensated per volume with SPM2 (Wellcome Department of Cognitive Neurology, London, UK), and head motion was corrected with rigid body translation and rotation with the FMRIB Software Library (FSL; Jenkinson et al. 2002; Smith et al. 2004). The data underwent further preprocessing specific to functional connectivity analysis, including low-pass temporal filtering, head-motion regression, whole brain signal regression, and ventricular and white matter signal regression (Van Dijk et al. 2010).

#### *Structural MRI Data Preprocessing and Functional-Structural Data Alignment*

Structural data preprocessing and functional-structural data alignment were the same as described in Yeo et al. (2011) and Buckner et al. (2011). The structural data were processed with automated algorithms provided in the FreeSurfer version 4.5.0 software package (<http://surfer.nmr.mgh.harvard.edu>), which reconstructed a surface mesh representation of the cortex from each individual subject's structural image and registered each subject to a common spherical coordinate system (Dale et al. 1999; Fischl et al. 1999a, 1999b, 2001; Ségonne et al. 2004, 2007). See Yeo et al. (2011) for details.

The structural and functional images were aligned (Fig. 1; similar to Buckner et al. 2011, Fig. 1, A and B) with boundary-based registration (Greve and Fischl 2009) available from the FsFast software package (<http://surfer.nmr.mgh.harvard.edu/fswiki/FsFast>). The resting-state BOLD fMRI data were then aligned to the common spherical coordinate system via sampling from the middle of the cortical ribbon in a single interpolation step (similar to Buckner et al. 2011, Fig. 1, A–C and E). Consistent with prior methods (Buckner et al. 2011; Yeo et al. 2011), a 6-mm full-width half-maximum (FWHM) smoothing kernel was applied to the fMRI data in the surface space and the data were downsampled to a 4-mm mesh. Examination of the nonsmoothed data revealed noisier but qualitatively similar parcellations as those from the smoothed data.

#### *Hybrid Surface- and Volume-Based Alignment*

The cerebral cortex was modeled as a two-dimensional surface to respect its topology and registered to a common spherical coordinate system, as described above. The striatum was modeled as a volume and aligned with a nonlinear volumetric registration algorithm in a process analogous to that done for the cerebellum in Buckner et al. (2011) (see their Fig. 1, B and D). For each subject, the structural volume was jointly deformed to a probabilistic template and segmented into one of multiple brain structures (Fischl et al. 2002, 2004; see Buckner et al. 2011 for more details). The resulting deformation field, together with the correspondence between the structural-functional data alignment discussed above, was used to transform the subject's fMRI data into the common FreeSurfer nonlinear volumetric space. The normalized volumetric fMRI data within the striatum (defined with a FreeSurfer template mask of the striatum; we note that the tail of the caudate is not included in this mask) were smoothed with a 6-mm FWHM smoothing kernel. The use of this nonlinear deformation resulted in improved intersubject anatomical alignment (Fig. 2) compared with a linear transformation. The normalized FreeSurfer nonlinear volumetric data were transformed into FSL Montreal Neurological Institute (MNI) space (similar to Buckner et al. 2011, Fig. 1, D and E) with the spatial correspondence established by running the FSL MNI152 template (Fonov et al. 2011) through the FreeSurfer pipeline.

#### *Quality Control*

Registered functional and structural data were visually inspected for proper registration. Figure 1 shows good correspondence between the T1 and T2\* registration within the native space for three typical subjects (similar to Buckner et al. 2011, Fig. 1, A and B). Intersubject volumetric registration was also inspected for proper alignment of the striatum across subjects (similar to Buckner et al. 2011, Fig. 1, B and D). Figure 2 illustrates this with normalized T1 images for three typical subjects.

#### *Mapping Between Surface- and Volume-Based Coordinates and Visualization*

Spatial correspondence between the FreeSurfer surface and volumetric coordinate systems was established by averaging over 1,000 subjects the composition of the transformation from each subject's native space to the FreeSurfer surface space and the transformation from the FreeSurfer nonlinear volumetric space. Using the spatial correspondence between FSL MNI152 space and FreeSurfer nonlinear volumetric space, we were able to estimate MNI atlas coordinates (Evans et al. 1993; Fonov et al. 2011). All analyses were performed in FreeSurfer surface and volumetric spaces and displayed in MNI atlas space for the volume and the left and right inflated PALS cortical surfaces using Caret software (Van Essen 2005) for the surface.

#### *Regression of Adjacent Cerebral Cortex Signal When Analyzing the Striatum*

The physical proximity of the striatum to the insula and orbital frontal cortices resulted in the blurring of fMRI signal at the cortical-striatal boundary, particularly between the putamen and insula. To eliminate the cortical signal, we regressed out the mean signal of the cortical voxels that were within 4.0 (8 mm) or 4.5 (9 mm) voxels from the left or right putamen, respectively (see Buckner et al. 2011 for use of this general approach for the cerebellum). The distances were asymmetric to allow for approximately equal numbers of left and right cortical voxels to contribute to the regression. The regression took place on the individual subject level: the fMRI signals within the left and right cortical regression masks were averaged and regressed out from the smoothed fMRI data within the striatum.

#### *Signal-to-Noise Ratio Maps*

Temporal SNR of the motion-corrected fMRI time series was computed for each voxel in the subject's native volumetric space by averaging the signal intensity across the whole run and dividing it by the standard deviation over time. The SNR was averaged across runs within subject when multiple runs were available. The SNR was then averaged across the 1,000 subjects from the core data set and displayed in the volume to visualize the SNR of the striatum (Fig. 3). SNR was good throughout most of the striatum; signal dropout occurred primarily in and around the ventral striatum/nucleus accumbens. Another issue to keep in mind is that there may be insufficient power to accurately characterize striatal regions that are coupled to cerebral regions with low SNR, such as the orbital frontal cortex (see Fig. 3 of Yeo et al. 2011).

#### *Striatum Parcellation and Confidence Maps*

Unlike the cerebellum, which has relatively specific functional connectivity correlations to cerebral networks, the striatum has less specific correlations that in some places spill across cortical network boundaries (see Fig. 11 for illustration), which may be due to the higher impact of signal blurring on the structurally smaller striatum. For this reason, using the method employed for the cerebellum parcellation (Buckner et al. 2011) leads to striatal voxel assignments

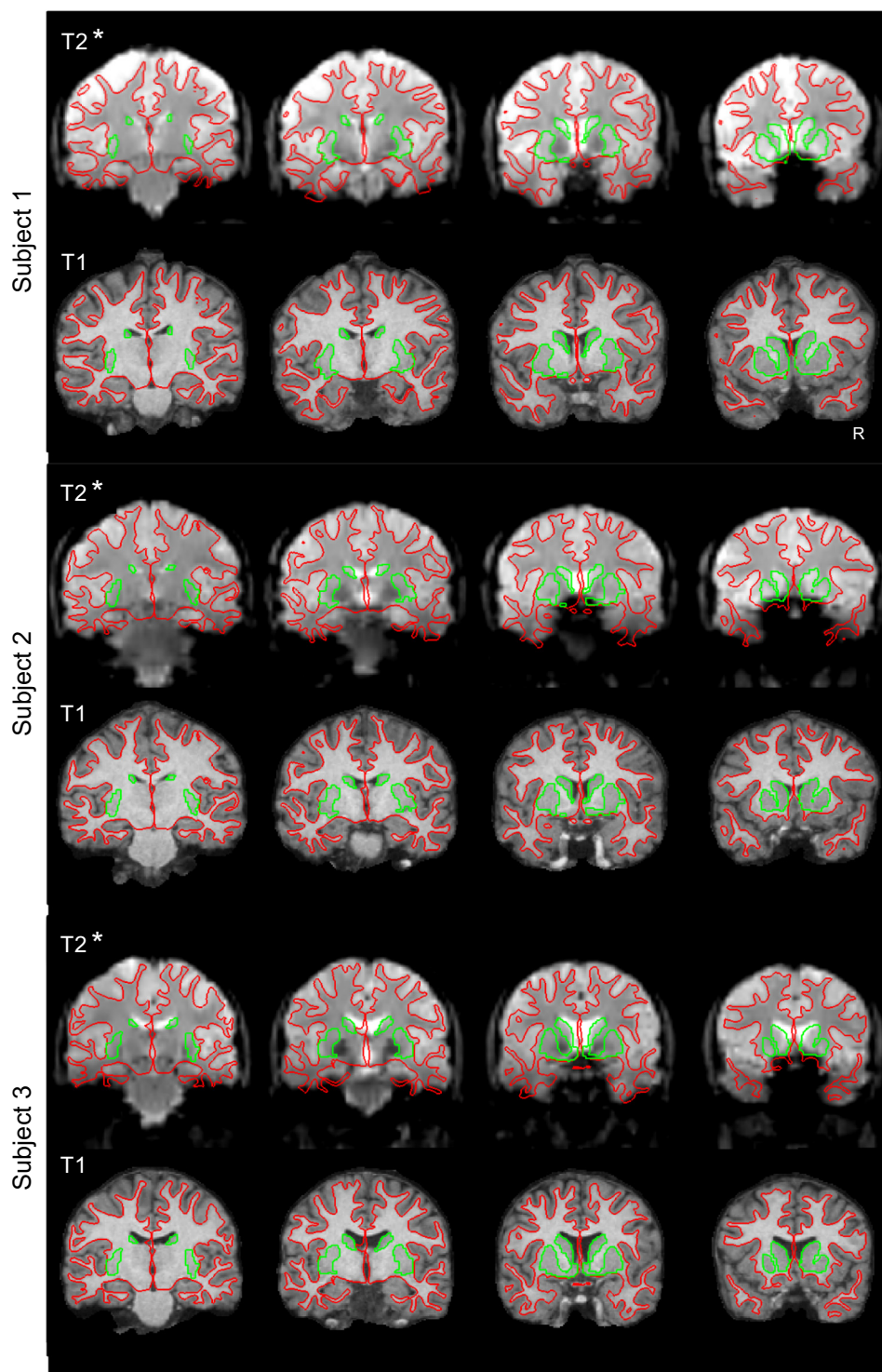


**Fig. 1.** Examples of within-subject surface and volume extraction. Examples of the extracted cerebral cortex surface and striatal boundaries are shown for 3 typical subjects within their native space. The red line delineates the estimated boundary of the cerebral cortical surface between the gray and white matter. The green line shows the estimated edge of the striatum tailored to each individual subject's T1-weighted image. The green line is superimposed on the T2\* images to illustrate deviations in the blood oxygenation level-dependent (BOLD) data. Imperfections are apparent in the BOLD data, particularly in the ventral striatum, which lies near to the signal dropout region of the orbital frontal cortex.

that, upon examining the underlying functional connectivity, do not reflect the strongest correlations of that voxel. For example, voxels in the ventral putamen ( $y = -7$ ) were assigned to the default network because of extensive low-level correlations to regions of the default network, even though the strongest correlations resided in the motor network. To create parcellations representing the most strongly correlated network, we chose an alternative method of parcellation for the striatum. For each striatal voxel, the top 25 most correlated cortical vertices were selected and the network with the most vertices belonging to it became the assigned network for the striatal voxel. For example, within the top 25 cortical vertices for a striatal voxel, if 13

resided in one network and 12 in another, that striatal voxel would be assigned to the first network; 25 was selected as the number of top cortical vertices to use because this led to parcellations that most accurately reflected the strongest underlying correlations. This approach mostly affected the ventral putamen at around  $y = -7$ , with a portion of the striatal voxels switching from default (red) to motor (blue) assignment. Since striatal voxels varied on how well they belonged to their assigned networks, a confidence map was calculated in which the fraction of the top 25 correlated cortical vertices belonging to the assigned network was computed for each striatal voxel (e.g., in the above example of a striatal voxel with 13 vertices in the

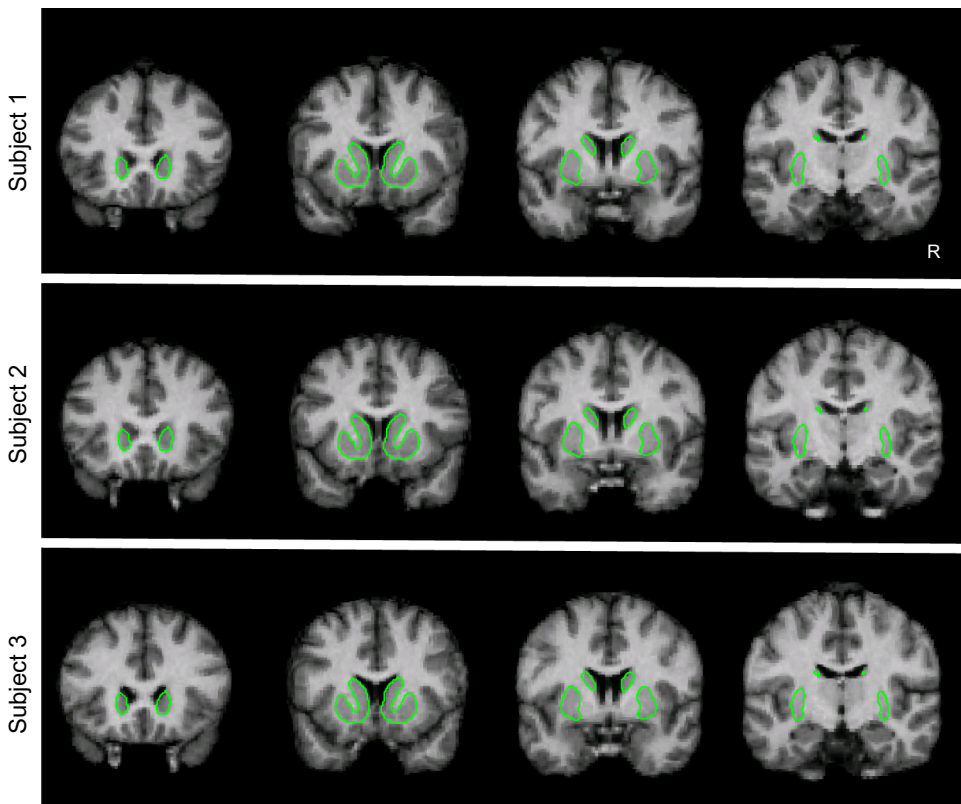


**Fig. 2.** Examples of between-subject striatal alignment. Volumetric images are shown for the registered structural data from 3 typical subjects. The green line represents the striatal edge estimated from the group structural template and is superimposed identically across the subjects to illustrate each individual's registration to the group template. Each subject's striatum is well registered in relation to the template. Close examination reveals subtle differences between subjects reflecting alignment errors on the order of a few millimeters.

first-choice network and 12 vertices in the second-choice network, the confidence value =  $13/25 = 0.52$ ).

#### Seed Region Correlation Estimates Between the Striatum and Cerebrum

Striatal fcMRI maps for specific cerebral seed regions were obtained by computing the Pearson's product-moment correlation between the surface region's preprocessed resting fMRI time course and the time courses of striatal voxels. Each cerebral seed region included a single surface vertex ( $\sim 4 \times 4 \text{ mm}$ ) but should be considered spatially more extensive because of spatial smoothing. Conversely, a correlation map from each striatal seed region was obtained by computing the correlation between the voxel's time course and the time courses of all vertices on the cerebral cortical surface. Striatal seed regions were restricted to a single voxel ( $2 \times 2 \times 2 \text{ mm}$ ) and affected by spatial smoothing. To obtain group-averaged correlation  $z$  maps, the correlation maps of individual subjects were converted to individual subject  $z$  maps with Fisher's  $r$ -to- $z$  transformation and then averaged across all subjects in the group. Fisher's  $r$ -to- $z$  transformation increases normality of the distribution of correlations in the sample. For subjects with multiple runs, the individual subject  $z$  maps were first averaged within the subject before submitting to the group average. An inverse Fisher's  $r$ -to- $z$  transformation was then applied to the group-averaged correlation  $z$  map, yielding a group-averaged correlation map.

#### Selecting Regions for Functional Connectivity Analysis

The striatal fcMRI maps of the foot and tongue representations (see Fig. 4B) were created with cerebral seed regions corresponding to the foot and tongue representations in the motor cortex based on an fMRI motor task as described by Buckner et al. (2011). The foot and tongue single voxel striatal seed regions (Fig. 4B) were chosen from these maps from regions that had strong and minimally overlapping foot and tongue correlations. These seed regions

were used to create cortical fcMRI maps from the foot and tongue representations in the striatum (Fig. 4C). Seed region coordinates are reported in Table 1.

The striatal fcMRI maps of the SMA and motor hand representations (see Fig. 5B) were created with cerebral seed regions corresponding to the SMA and the hand representation in the motor cortex based on an fMRI motor task from Buckner et al. (2011). The hand region of the motor cortex was chosen to approximately match the monkey anatomical cases shown (Fig. 5A), in which injections were made in the forelimb regions of the ipsilateral primary motor cortex and SMA of the monkey. The selection of the SMA seed region was guided by the probabilistic histological map of BA6 created from 10 human subjects (Fischl et al. 2008; Geyer 2004). The seed region was selected to be posterior to the anterior commissure, which is suggested by Picard and Strick (1996) to be a rough anatomical boundary line between the pre-SMA and SMA. Single voxel striatal seed regions (Fig. 5B) were selected within the striatal fcMRI maps derived from the cerebral SMA and the motor hand seed regions and used to create cortical fcMRI maps (Fig. 5C).

In Fig. 10, *seed region A* in the motor zone (blue) was the same as the striatal tongue seed region used in Fig. 4. *Seed region B* was selected to be in a relatively high-confidence region of the default network zone (red) of the posterior ventral striatum.

The striatal seed regions in Fig. 11 are representative of their respective networks and selected from high-confidence regions (Table 2). The cerebral seed regions in Fig. 12 were selected to consist of multiple seed regions each from the default (red), frontoparietal control (orange), ventral attention (violet), and dorsal attention (green) networks, with two or three anterior (frontal) and one or two posterior seed regions, as well as one seed region from the limbic network (cream; Table 2). The cerebral seed regions in Fig. 18 (see Table 4) were placed in distributed regions of the association networks of the 17-network parcellation labeled in red and yellow. Seed regions from Yeo et al. (2011) were used for aMT+, IPS3<sub>m</sub>, PFC<sub>la</sub>, PFC<sub>da</sub>, PFC<sub>dp</sub>, PCC, PFC<sub>m</sub>, PFC<sub>mp</sub>, PFC<sub>v</sub>, PGa, PrC<sub>v</sub>, and FEF. The remaining seed

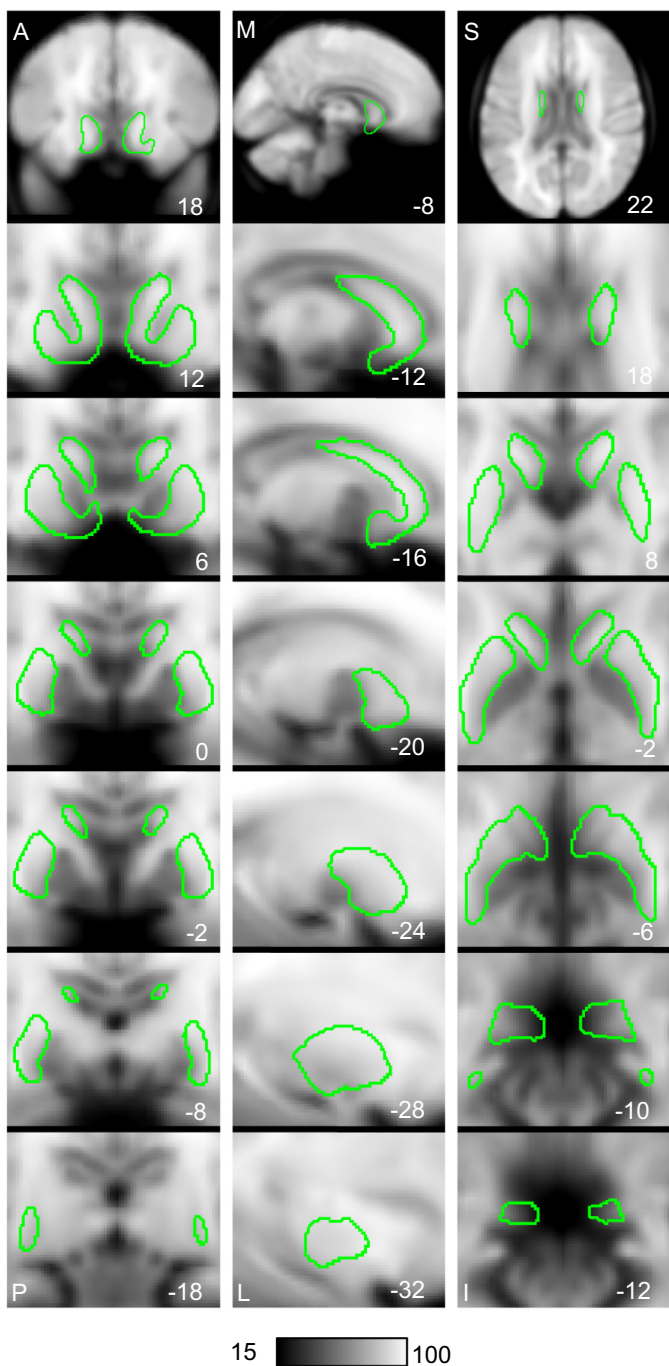


Fig. 3. Signal-to-noise ratio (SNR) maps of the functional data from the full sample ( $N = 1,000$ ). The mean estimate of the BOLD fMRI data SNR is illustrated for coronal (left), sagittal (center), and transverse (right) images. The sagittal sections are of the left hemisphere. A, anterior; P, posterior; M, medial; L, lateral; S, superior; I, inferior. The slice coordinate in the MNI atlas space is located at the bottom right of each panel. The estimate of the striatal edge from the group template is illustrated in green (similar to Fig. 2). Note the generally high and uniform SNR except for regions of ventral striatum.

regions were selected to cover other key cerebral regions. PF<sub>v</sub>, PGa<sub>v</sub>, PGc, PG<sub>dp</sub>, PrCO, and 6<sub>am</sub> were labeled based on probabilistic histological maps of nearby areas (Caspers et al. 2006; Fischl et al. 2008; Geyer 2004). Seed region subgenual cingulate area 25 (scg25), which lies in the limbic (cream-colored) cortical network, was based on the peak scg25 coordinate from a GingerALE meta-analysis of fMRI studies (Fitzgerald et al. 2008) reporting the responses of

Table 1. Locations of seed regions used to assess specificity of somatomotor and ventral attention networks

	Left Hemi Coordinates
Cerebral Cortex	
M1 <sub>F</sub> (foot)	-6, -26, 76
M1 <sub>H</sub> (hand)	-41, -20, 62
M1 <sub>T</sub> (tongue)	-55, -4, 26
SMA	-3, -5, 59
Striatum	
Motor foot	-29, -9, 8
Motor hand	-30, -7, 2
Motor tongue	-29, -9, -5
SMA	-24, -7, 7
Ventral striatum (default zone)	-28, -9, -10

Coordinates represent  $x$ ,  $y$ ,  $z$  in the atlas space of the Montreal Neurological Institute (MNI). Motor task fMRI together with probabilistic histological maps of areas 2 and 4 (Fischl et al. 2008; Geyer et al. 1996; Grefkes et al. 2001) were used to identify foot, hand, and tongue regions of the motor cortex (M1<sub>F</sub>, M1<sub>H</sub>, M1<sub>T</sub>) in the left hemisphere. A probabilistic histological map of area 6 (Geyer 2004) and a comparison of monkey and human motor tasks (Picard and Strick 1996) were used to identify the supplementary motor area (SMA) in the left hemisphere. All striatal seed regions were selected in regions with strong and specific correlations from their respective cortical functional connectivity maps. The ventral striatum seed region was placed in a relatively high-confidence region of the default network zone in the posterior ventral striatum.

depressed patients to positive stimuli, such as happy faces. Coordinates reported in the Talairach and Tournoux (1988) coordinate system (2.62, 15.17, -3.42) were flipped to the left hemisphere and converted to MNI152 space (-2.65, 15.8, -3.16; Brett 1999). The closest MNI coordinates completely within our cortical brain mask were used (-3, 16, -7).

Table 2. Locations of seed regions used to quantify specificity of association and limbic networks

	Left Hemi Coordinates
Cerebral Cortex	
aMT+	-51, -64, -2
FEF	-26, -6, 48
IPS3 <sub>m</sub>	-31, -48, 46
PCC	-3, -49, 25
PF <sub>v</sub>	-55, -38, 33
PF <sub>da</sub>	-31, 39, 30
PFC <sub>dp</sub>	-44, 15, 48
PFC <sub>la</sub>	-41, 55, 4
PFC <sub>m</sub>	-7, 46, -2
PFC <sub>mp</sub>	-5, 22, 47
PGa	-52, -50, 49
PGc	-42, -61, 31
PrC <sub>v</sub>	-50, 6, 30
PrCO	-35, 7, 5
scg25	-3, 16, -7
6 <sub>am</sub>	-4, 9, 47
Striatum	
Frontoparietal control network	-12, 10, 8
Default network	-8, 10, 1
Limbic network	-10, 11, -9

Left hemisphere cerebral cortical seed regions were obtained from Yeo et al. (2011) except for precentral operculum (PrCO), anterior medial BA6 (6<sub>am</sub>), ventral area PF (PF<sub>v</sub>), and central area PG (PGc), which were selected from the discovery data set to cover remaining key cortical regions and named based on probabilistic histological maps of nearby areas (Caspers et al. 2006; Geyer 2004) and scg25, which was based on a metaanalysis of fMRI studies (see METHODS). Striatal seed regions were selected from the frontoparietal control, default, and limbic networks based on the discovery data set, with the confidence map as a guide.

The comparisons in Figs. 15–17 were selected as regions for which an approximate comparison could be made between monkey anatomical projections and human functional connectivity. Each region had at least two agreeing monkey tract-tracing cases from independent laboratories (Table 3). Our procedure for selecting regions is imperfect because of difficulties in assessing homologies and defining specific areal boundaries, especially in association cortex. Nonetheless, comparisons allowed us to make a qualitative assessment of whether broad organizational properties of the striatum in the monkey parallel those observed in the human.

In Fig. 15, the motor and SMA anatomical tracing estimates were from injections in the forelimb regions of the monkey motor cortex (Liles and Updyke 1985, Case Rhesus Monkey) and SMA (Inase et al. 1999, Case San). The corresponding human motor hand and SMA seed regions were the same as those used in Fig. 5. The PFC<sub>lp</sub> anatomical tracing estimate was from an injection in the dorsal bank of the principal sulcus (Yeterian and Pandya 1991, Case 6). The corresponding human PFC<sub>lp</sub> seed region (from Yeo et al. 2011) was located in the middle frontal gyrus and placed centrally to minimize the possibility of being in areas 10 or 8 (Petrides and Pandya 1999). The PFC<sub>md</sub> anatomical tracing estimate was from area 32 (Ferry et al. 2000, Case OM35). The corresponding human PFC<sub>md</sub> seed region

was placed at or near area 32, just anterior to the genu of the cingulate gyrus. The exact homology of these human and monkey area 32 regions is uncertain because of the expansion of the medial prefrontal cortex in the human and a putative anterior-posterior shift of macaque area 32 (Öngür et al. 2003; see also Buckner et al. 2008). This approximation may be sufficient at our resolution as the region just rostral to the anterior cingulate as well as the zone encompassing a portion of the subgenual anterior cingulate fall within the same functional connectivity network (Yeo et al. 2011). The scg25 anatomical tracing estimate was from an injection in area 25 (Haber et al. 2006). The corresponding human seed region was the same as the one described in the previous paragraph for seed region scg25.

In Fig. 16, seed regions were placed in distributed regions of a single association network, the frontoparietal control network (orange): PFC<sub>lp</sub>, PGa, and PFC<sub>mp</sub> (from Yeo et al. 2011). The anatomical tracings were from Selemon and Goldman-Rakic (1985): areas 9 and 10 (Case 1), area 7 (Case 11), and area 9 medial (Case 5), respectively. In Fig. 17, the STS anatomical tracing estimate was from an injection in area 22 (Selemon and Goldman-Rakic 1985, Case 12) on the anterior superior temporal gyrus. Because the extent of the expansion of the superior temporal pole in humans is unknown, the corresponding human STS seed region (from Yeo et al. 2011) was

**Table 3.** Seed regions and studies used to compare human functional connectivity and monkey anatomy

Cortical Region	Left Hemi Human Coordinates	Monkey Injection Site	Replicated Monkey Anatomical Studies
Motor foot	-6, -26, 76	Motor hindlimb	Case 72-451, Künzle 1975 Cases 32L, 37L, <b>40</b> , Flaherty and Graybiel 1993 Case 31R, Flaherty and Graybiel 1994
Motor hand	-41, -20, 62	Motor forelimb	Cases <b>Rhesus Monkey</b> , Cynomolgus Monkey, Liles and Updyke 1985 Case 42, Flaherty and Graybiel 1993 Cases O, M, Inase et al. 1996 Case <b>Ta</b> , Takada et al. 1998a Case <b>Si</b> , Takada et al. 1998b Case CMA7, Takada et al. 2001
Motor tongue	-55, -4, 26	Motor face or mouth	Case 72-448, Künzle 1975 Case <b>40</b> , Flaherty and Graybiel 1993
SMA	-3, -5, 59	SMA forelimb	Cases O, M, Inase et al. 1996 Cases <b>Ta</b> , It Takada et al. 1998a Case <b>Tk</b> , Takada et al. 1998b Case <b>San</b> , Inase et al. 1999 Cases CMA5, CMA6, Takada et al. 2001
PCC	-3, -49, 25	PCC or Rsp	Case SM-85, Powell 1978 Case <b>1</b> , Baleydier and Mauguire 1980
PFC <sub>a</sub>	-8, 69, 7	Area 10	Case 4, Yeterian and Pandya 1991 Case Area 15B, Eblen and Graybiel 1995 Cases OM36, <b>OM38</b> , Ferry et al. 2000
PFC <sub>lp</sub>	-45, 29, 32	Areas 9 or 46	Case <b>1</b> , Selemon and Goldman-Rakic 1985 Cases 5, <b>6</b> , Yeterian and Pandya 1991 Case 131, Calzavara et al. 2007
PFC <sub>md</sub>	-11, 45, 6	Area 32	Case <b>2</b> , Yeterian and Pandya 1991 Case <b>OM35</b> , Ferry et al. 2000
PFC <sub>mp</sub>	-5, 22, 47	Area 9m	Case <b>5</b> , Selemon and Goldman-Rakic 1985 Case 78, Calzavara et al. 2007
PGa	-52, -50, 49	Area 7	Case 1B, Yeterian and Van Hoesen 1978 Case <b>11</b> , Selemon and Goldman-Rakic 1985 Case 5, Cavada and Goldman-Rakic 1991 Case <b>2</b> , Cavada and Goldman-Rakic 1991 Cases 19, 22, Yeterian and Pandya 1993 Case OM32, Ferry et al. 2000
PGc	-42, -61, 31	Area 7a/Opt	Fig. 2, Haber et al. 2006 Fig. 2, Yeterian and Van Hoesen 1978 Case 4, Van Hoesen et al. 1981
scg25	-3, 16, -7	scg25	Case <b>12</b> , Selemon and Goldman-Rakic 1985 Case 5, Yeterian and Pandya 1998
STS	-55, -10, -16	Anterior superior temporal gyrus	

These cortical regions were selected for having a suspected homology between monkey and human and having at least 2 replicated monkey tract-tracing injection cases from independent laboratories. Human seed region coordinates were selected with a variety of methods, including human histological probability maps and human motor fMRI tasks. Cases listed in bold type were adapted with permission for use in Figs. 4, 5, 15, 16, and 17. See METHODS and figures for further details.

placed in the middle portion of the superior temporal sulcus that showed a similar pattern in the functional connectivity to the anatomy. The PGc injection was made in area 7a of the monkey (Cavada and Goldman-Rakic 1991, Case 2). The corresponding human seed region was placed in the inferior parietal lobule below the intraparietal sulcus, which is more likely to correspond to monkey area 7a or Opt. The PCC and PFC<sub>md</sub> injections were in area 23/PCC (Baleydier and Mauguiere 1980, Case 1) and area 32 (Yeterian and Pandya 1991, Case 2), respectively; the corresponding human seed regions were the same as those described for Figs. 12 and 15, respectively. Finally, the frontal pole injection was in area 10o (Ferry et al. 2000, Case OM38). The human frontal pole seed region (PFC<sub>a</sub>) was placed in the medial aspect of estimated area 10p (Öngür et al. 2003), anterior to the PFC<sub>md</sub> seed region.

The cortical seed region ( $-40, 4, -2$ ) used to create the fcMRI maps in Fig. 13 was placed in the ventral attention network (violet) portion of the insula in the 7-network parcellation in order to illustrate the cortical signal bleeding into the striatum.

#### Distribution of Parcellations and Raw Data

A primary result of our analyses is the parcellation of the striatum into networks. The parcellations in FreeSurfer space are available ([http://www.freesurfer.net/fswiki/StriatumParcellation\\_Choi2012](http://www.freesurfer.net/fswiki/StriatumParcellation_Choi2012)). Movies of the region-based functional connectivity estimates can be downloaded from <http://www.youtube.com/choyeobuckner>. The raw fMRI data from the 1,000 subjects in the functional connectivity analysis will be made openly available to researchers using the procedures established by the OASIS data releases (Marcus et al. 2007, 2010) and the 1,000 Functional Connectomes Project (Biswal et al. 2010).

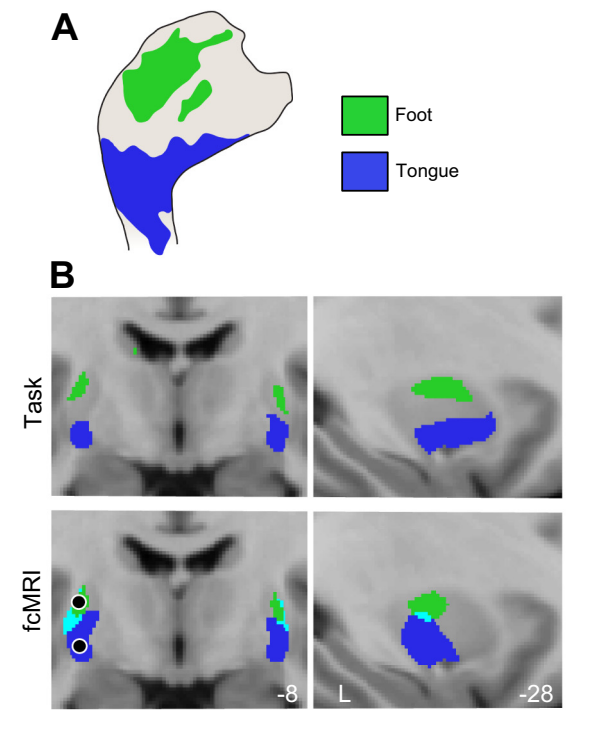
## RESULTS

### Functional Connectivity Reveals Somatomotor Topography of the Striatum

Anatomical tract-tracing (Flaherty and Graybiel 1993; Künzle 1975) and electrophysiological studies (Alexander and DeLong 1985) have shown that the primary motor cortex projects to the putamen with an inverted topography. Figure 4A shows a representative tract-tracing case (Flaherty and Graybiel 1993) of the foot and tongue in the monkey putamen. The same inverted topography was seen in the human striatum with an fMRI motor task conducted in our companion paper (Buckner et al. 2011; Fig. 4B), in which subjects moved their feet or tongues. Functional connectivity revealed the inverted motor topography (Fig. 4B; discovery sample). fcMRI maps of seed regions placed in the striatal foot and tongue representations (Table 1) show that cerebral correlations are specific to their respective motor cortex representations (Fig. 4C; replication sample). These results demonstrate that functional connectivity identifies the expected inverted somatomotor topography in the striatum.

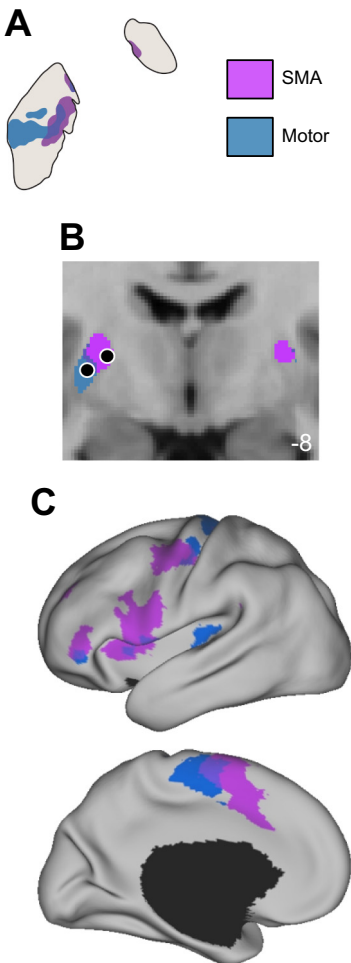
### Functional Connectivity Reveals Lateral-Medial Division of Primary Motor and Supplementary Motor Cortices in the Striatum

Figure 5A shows a representative case of a double injection in the hand regions of the ipsilateral primary motor cortex (M1) and SMA in one monkey (Takada et al. 1998a). The tracing shows that the SMA preferentially projects medially and the primary motor cortex projects laterally to one another in the monkey putamen (for ipsilateral areas). Seed regions in the estimated human homolog of SMA and the hand-specific region of the motor cortex (Table 1) correlate preferentially to the medial and



**Fig. 4.** Functional connectivity reveals the inverted somatomotor topography within the posterior putamen that is comparable to monkey anatomy and task-evoked estimates. *A*: a representative case of the inverted somatomotor topography in the monkey putamen revealed by tracer injections in the foot (green) or tongue (blue) representation of the primary motor cortex. Adapted from Flaherty and Graybiel (1993) with permission (see Table 3 under Motor foot). *B*: coronal sections (*left*,  $y = -8$ ) and left sagittal sections (*right*,  $x = -28$ ) display the inverted somatomotor topography in the task-evoked (*top*) and functional connectivity (*bottom*) data. Green color indicates foot representation; blue color indicates tongue representation. The functional connectivity images were produced from the replication sample ( $n = 500$ ) using seed regions in the foot- and tongue-specific motor cortex representations from the task-evoked data. *C*: functional connectivity from the foot- and tongue-specific representations in the putamen (seed regions shown in *B*, *bottom*) show specific correlations with the foot and tongue regions of the motor cortex. A threshold of 0.4 was used for the task data,  $z(r) > 0.035$  for the motor foot and  $z(r) > 0.045$  for the motor tongue striatal functional connectivity MRI (fcMRI) data, and  $z(r) > 0.09$  for the cortical fcMRI data. Seed region coordinates are reported in Table 1. Monkey corticostriatal projection tracings shown here and in subsequent figures were redrawn for conformity. Original tracings showed terminal labeling; redrawings included both dense and diffuse projections. Original tracings of the right striatum were flipped in the redrawings for conformity.

lateral putamen, respectively (Fig. 5B; discovery sample). Cortical fcMRI maps derived from seed regions in the striatal motor and SMA representations (Table 1) showed preferential correlations to the primary motor cortex and SMA, respectively (Fig. 5C; replication sample). The SMA correlations, however, were not specific, possibly because of signal bleeding between the putamen and the adjacent cortex, which we discuss further below.



**Fig. 5.** Functional connectivity reveals the lateral-medial topography of the primary motor and supplementary motor cortices within the putamen that is comparable to monkey anatomy. *A*: a representative case of the lateral-medial topography of the primary motor cortex and supplementary motor area (SMA) in the monkey putamen revealed by tracer injections in the motor (blue) and SMA (purple) forelimb representations. Adapted from Takada et al. (1998a) with permission (see Table 3 under SMA). *B*: a coronal section ( $y = -8$ ) displays the lateral-medial topography in the functional connectivity data produced from the replication sample ( $n = 500$ ) using seed regions of the task-evoked motor hand representation and the estimated human SMA homolog. Thresholds of  $z(r) > 0.04$  and 0.09 were applied for the motor hand and estimated SMA striatal fMRI maps, respectively. *C*: functional connectivity maps from the motor- and SMA-specific striatal seed regions (regions shown in *B*) illustrate their preferential correlations with primary motor cortex and SMA. A threshold of  $z(r) > 0.07$  was applied. Seed region coordinates are reported in Table 1. Note that there is also correlation with insular regions that fall near to the striatum. We suspect that these are residual artifacts of limited resolution that are not fully handled by our methods (see text).

#### *Functional Connectivity Reveals a Complete Functional Map of the Striatum*

The reasonable agreement between the monkey anatomical studies and functional connectivity for motor cortex suggested that functional connectivity could be used to map the striatum comprehensively. Our mapping strategy entailed assigning each striatal voxel to its most strongly correlated cortical network (see METHODS) in the 7- and 17-network cortical parcellations, as identified by Yeo et al. (2011). Figure 6 shows the high degree of reliability (7-network: 90.2%, 17-network: 87.1% overlapping voxels) of this method in two independent sets of 500 subjects

(discovery and replication) for both parcellations. Disagreement between the discovery and replication samples tended to be between neighboring networks, especially within association cortex [e.g., 81.1% of the voxel disagreements for regions falling within the default network (red) in the discovery sample were classified to the frontoparietal control network (orange) in the replication sample]. Figures 7 and 8 display best estimates of the 7- and 17-network parcellations using all 1,000 subjects. Figure 9 shows the confidence estimates of the parcellations.

Several observations emerged from these parcellations. First, the 7-network striatal parcellation (Fig. 7) showed that five of the seven networks are strongly represented in the striatum: motor (blue), ventral attention (violet), frontoparietal control (orange), default (red), and limbic (cream) networks. There was a small representation of the dorsal attention (green) network in the right posterior ventral putamen and virtually no representation of the visual (purple) network. The 17-network parcellation (Fig. 8) appeared to be a fractionation of the 7-network parcellation with a similar pattern but with finer-grain information about functional divisions within a network. One notable exception to this is the pink network at around  $y = 12$ , which is a region susceptible to cortical signal bleeding as we discuss below.

Second, the assignments of the motor (blue) network and the ventral attention (violet) network, which includes premotor areas, in the 7-network parcellation agreed with the cerebral cortex fMRI analyses shown in Figs. 4 and 5. The posterior putamen was assigned to the motor network laterally and the ventral attention network medially. Furthermore, the motor representation in both the motor cortex and striatum fractionated into dorsal foot (blue) and ventral tongue (aqua) parcellations in the 17-network model, consistent with the inverted somatotopy seen in monkey anatomy. These results suggest that the parcellation method recovers the topographic arrangements of motor subdivisions.

Third, the parcellations broadly agree with prior models of the striatum that propose gradients of connectivity. The 7-network parcellation shows that corticostriatal circuits, in particular the association circuits, couple to zones of the striatum that extend along its longitudinal extent, consistent with anatomical studies (Selemon and Goldman-Rakic 1985; Yeterian and Van Hoesen 1978). There is also a dorsolateral to ventromedial organization (Haber et al. 1994; Parent 1990; Parent and Hazrati 1995). We expand on these organizational properties in DISCUSSION.

Fourth, the parcellation parallels monkey anatomical projections in the posterior ventral striatum. In addition to projections to the ventral putamen from the tongue region of the motor cortex, monkey anatomy reveals projections to the posterior-most portion of the ventral striatum from association and limbic cortices [there are also projections from subcortical structures, such as the amygdala (Fudge et al. 2002, 2004; Russchen et al. 1985), but we will not address them here]. Figure 10 shows the 7-network parcellation of the posterior ventral striatum and the corresponding fMRI maps, showing that the posterior ventral striatum is functionally coupled to the motor and, further ventrally, association cortical networks.

#### *Quantitative Measurement of Association and Limbic Corticostriatal Circuits Demonstrates Specificity*

The previous analyses illustrated that the functional connectivity of the motor cortex and SMA within the striatum is

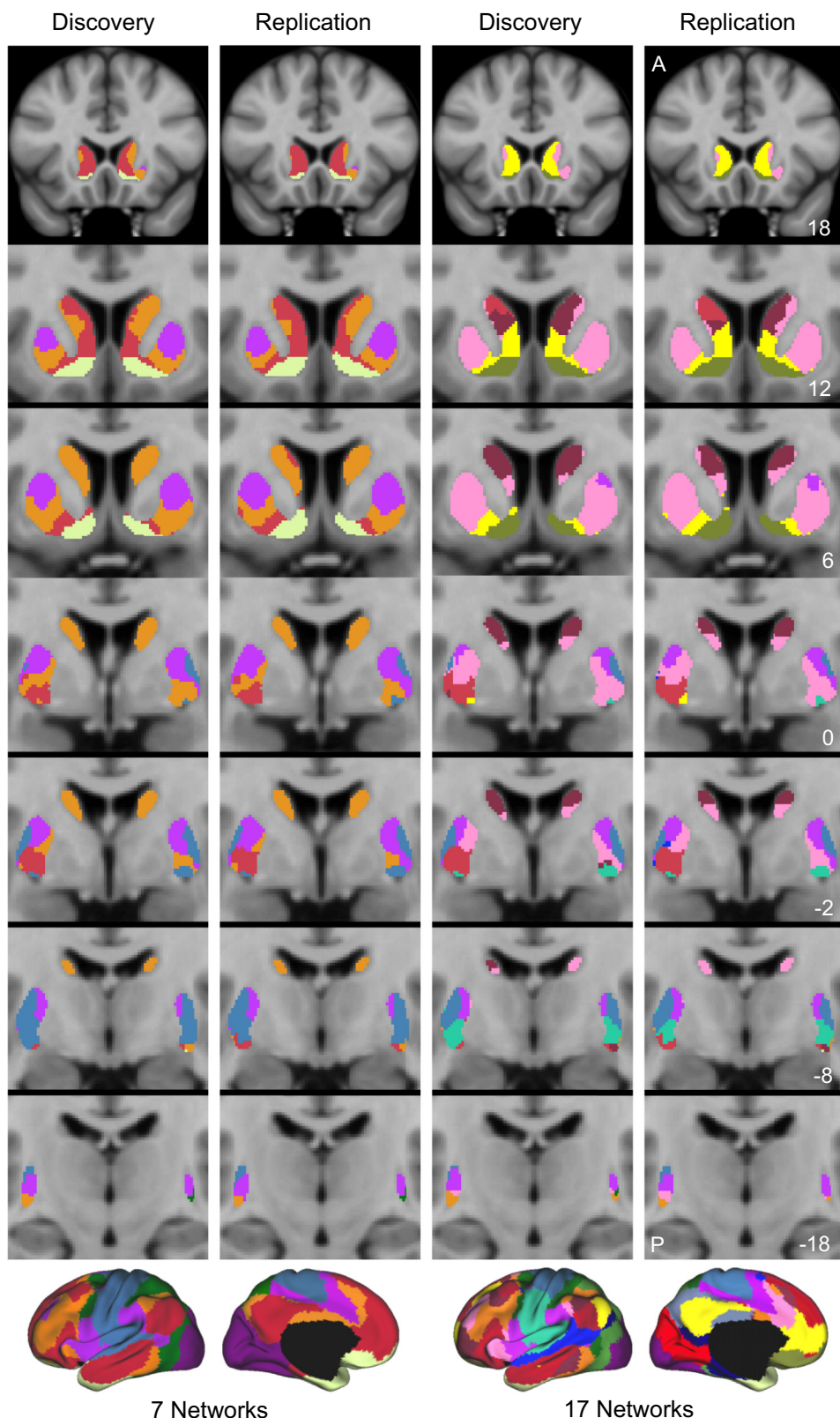


**Fig. 6.** Reliability of human striatal maps based on functional connectivity. Each voxel in the striatum is assigned a color corresponding to its most strongly correlated cerebral network according to the legends below of the 7 (*left*-) and 17 (*right*-) network cortical parcellations (from Yeo et al. 2011). The 7- and 17-network parcellations were each produced in the discovery sample ( $n = 500$ ) and replicated in the replication sample ( $n = 500$ ). For example, the blue regions of the striatum include those voxels that are more strongly correlated with the blue cerebral network (involving somatosensory and motor cortices) than any other network. Note that the discovery and replication maps are highly similar (voxel overlap was 90.2% and 87.1% for the 7- and 17-network estimates, respectively).

correctly localized in the 7- and 17-network striatal parcellations. We next sought to determine how well the parcellations captured seed-based functional connectivity estimates. Figure 11 shows the cortical fcMRI maps (replication sample) resulting from seed regions placed in high-confidence regions of the frontoparietal

control, default, and limbic divisions of the 7-network striatal parcellation (discovery sample; Table 2). These fcMRI maps revealed distinct correlation maps that largely agreed with the parcellation. For example, a region located in the central caudate head (*region A*) was correlated to cortical regions in

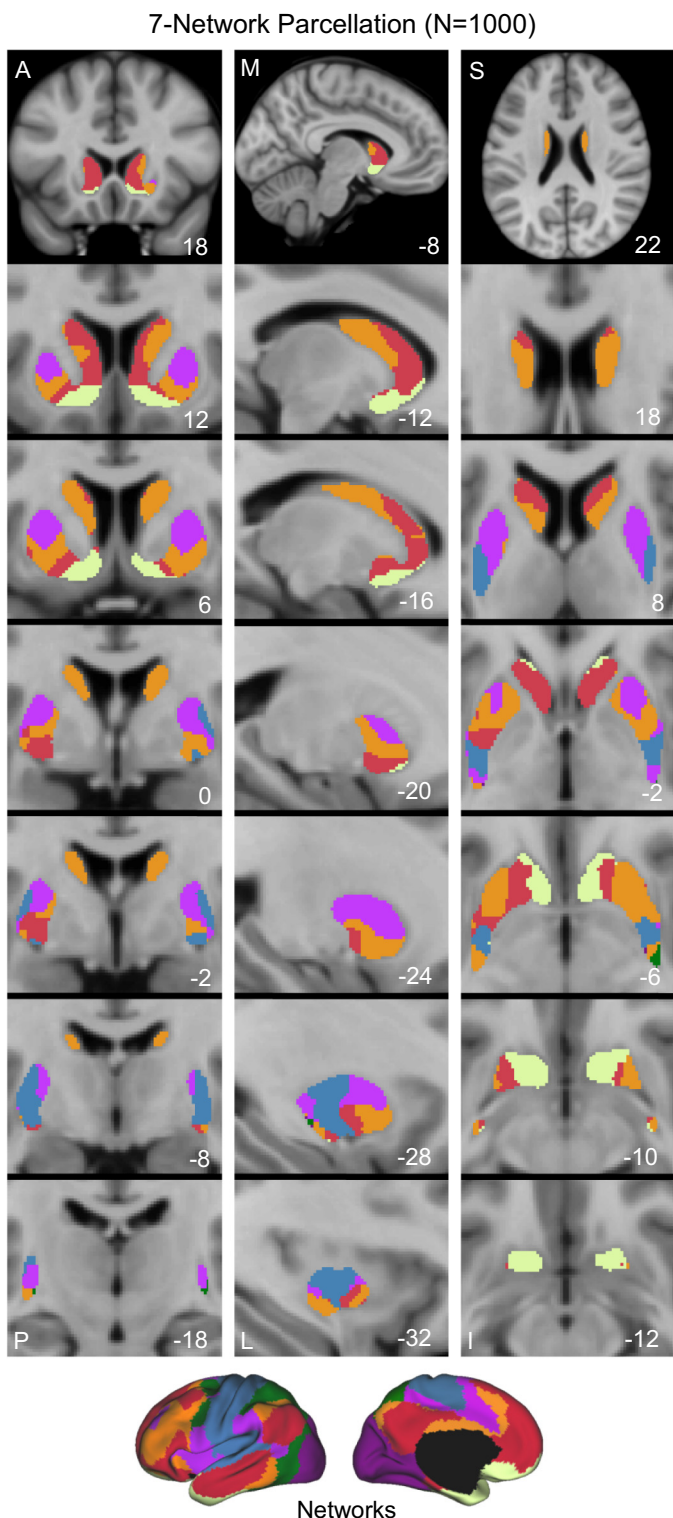


Fig. 7. A map of the human striatum based on functional connectivity to 7 major networks in the cerebrum. Each voxel in the striatum is assigned a color corresponding to its most strongly correlated cerebral network in the 7-network cortical parcellation shown at bottom (from Yeo et al. 2011). The full sample of 1,000 subjects was used to create a best estimate of the map. The sections display coronal (left), sagittal (center), and transverse (right) images. A, anterior; P, posterior; M, medial; L, lateral; S, superior; I, inferior. The slice coordinate in the MNI atlas space is located at the bottom right of each panel.

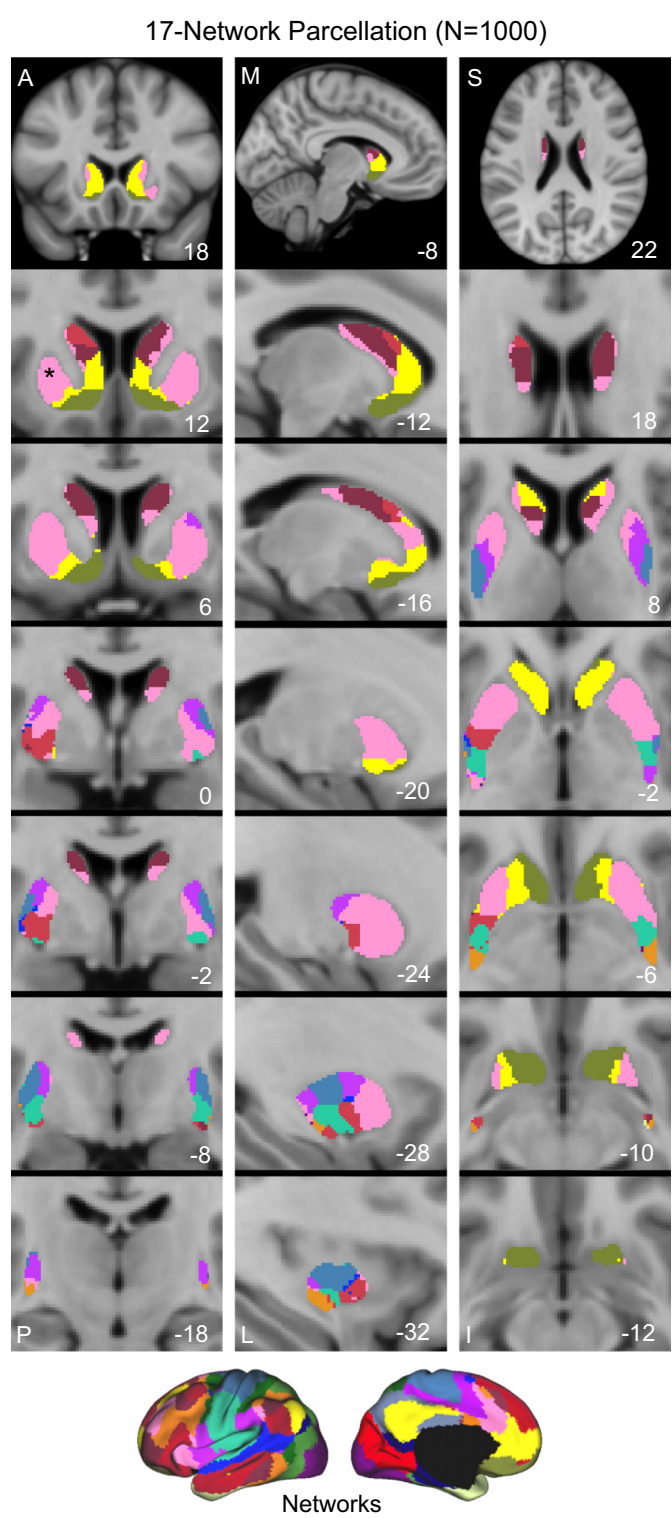


Fig. 8. A fine-parcellated map of the human striatum based on functional connectivity to 17 networks in the cerebrum. The format and use of abbreviations are the same as in Fig. 7 but in this instance in relation to a finer cerebral parcellation involving 17 networks (from Yeo et al. 2011). These data are from the full sample of 1,000 subjects. Note that this method identifies the correct locations of the foot (blue) and tongue (aqua) regions in the posterior putamen. As discussed in the text, some features of the parcellation are uncertain, as illustrated by the asterisk in the putamen (labeled as the pink network).

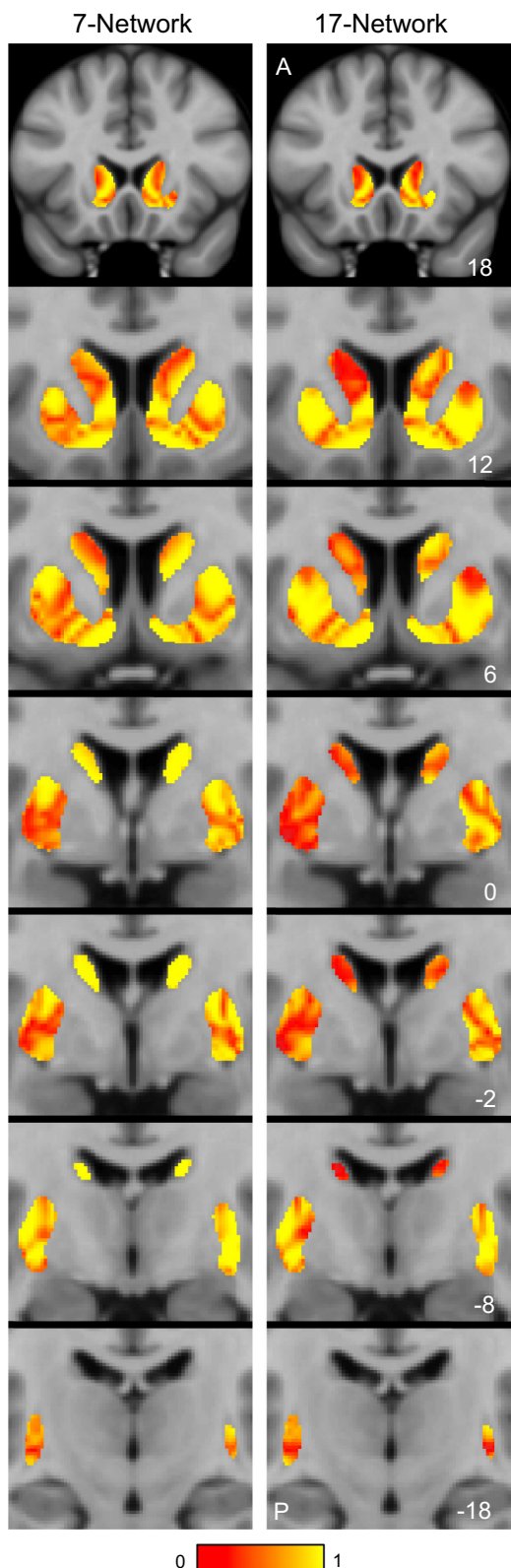


Fig. 9. Confidence of the parcellation estimates. Confidence values for each voxel of the striatum with respect to its assigned network vs. second-choice network are displayed for the 7 (left)- and 17 (right)-network estimates from 1,000 subjects. Network boundaries are generally associated with lower confidence values.

the frontoparietal control network, including the dorsolateral prefrontal cortex and the inferior parietal lobule (Fig. 11A). In contrast, a more ventral region (*region B*) was correlated to cortical regions linked to the default network, including the posterior cingulate cortex and medial prefrontal cortex (Fig. 11B). We note, however, that the cortical correlations did not always fall neatly within their assigned cortical networks: the correlations in some locations spilled across boundaries into neighboring networks or did not cover the entire assigned network. The latter patterns may be due to the resolution limitations or the presence of subnetworks, as we will explore later.

To quantitatively characterize the specificity of these corticostratal coupling patterns, we computed the correlations of the three striatal seed regions with cortical seed regions distributed throughout the cerebral cortex (Table 2). The results, plotted in polar form (Fig. 12), revealed three distinct functional connectivity patterns in which striatal seed regions were preferentially correlated to the cortical seed regions of their respective networks.

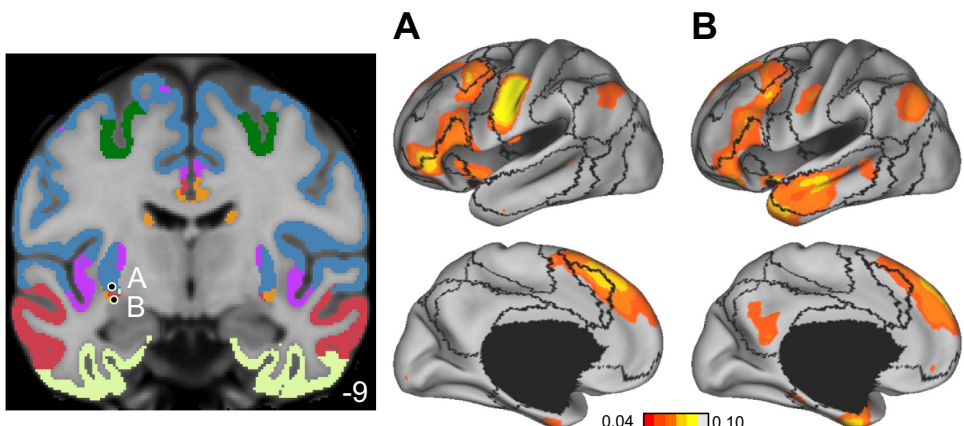
#### Cortical Signal Bleeding

Because of the proximity of the insula to the striatum, we suspected that there might be bleeding of cortical signal into the striatum. Signal bleeding has previously been observed between proximal structures, such as the visual cortex and the cerebellum (Buckner et al. 2011) and the sensorimotor and auditory cortices (Yeo et al. 2011). In the former case, regressing out the visual cortex signal from the cerebellum revealed correlations to the motor cortex, as predicted by monkey anatomical tract-tracing studies (Buckner et al. 2011). In the striatum, prior to regressing out the cortical signal, the majority of the putamen was assigned to the ventral attention network (violet) located adjacently in the insula (Fig. 13, A and E). This is most likely due to the strong correlations between the insula and the putamen as shown by an fMRI map of a seed region in the ventral attention network of the insula (Fig. 13, B and F; see METHODS for seed region coordinate). To correct for the signal bleeding, we regressed out the cortical signal within 8 or 9 mm of the striatum (see METHODS). This regression removed most of the correlations in the posterior putamen (Fig. 13D), leading to the assignment of the posterior putamen to the motor network (Fig. 13C), as predicted by monkey anatomy. In the anterior putamen, regressing out the proximal cortical signal reduced these correlations (Fig. 13H) and revealed the assignment of the central and ventral anterior putamen to the frontoparietal control and default networks (Fig. 13G), which also agrees with monkey anatomical tract-tracing studies (see Figs. 15–17).

We also examined an alternative regression method (Fig. 14) that removed the signal from only the neighboring cortical voxels (within 9 mm) of each striatal voxel, thus regressing out a unique signal for each striatal voxel. This revealed a parcellation (Fig. 14B) with slight shifts in network boundaries in these regions of uncertainty, but largely qualitatively similar to the first regression model (Fig. 14A).

These regression methods revealed that the putamen is susceptible to signal bleeding from the adjacent cerebral cortex. In contrast, the network assignments in the caudate remain

Fig. 10. Distinct regions of the posterior ventral striatum are coupled to motor and association cortical networks. Seed regions placed in the motor (*A*) and default (*B*) network assignments of the left posterior ventral striatum in the 7-network parcellation reveal correlation with the motor and default cortical networks, respectively, in the replication sample ( $n = 500$ ). The 7-network cortical parcellation is also displayed to show that these corticostriatal fcMRI correlations are minimally influenced by signal bleeding from the adjacent cortex.



qualitatively unchanged between the no-regression and regression methods. We are therefore least confident of the results in the putamen and will focus on the more certain caudate results in the remainder of this report.

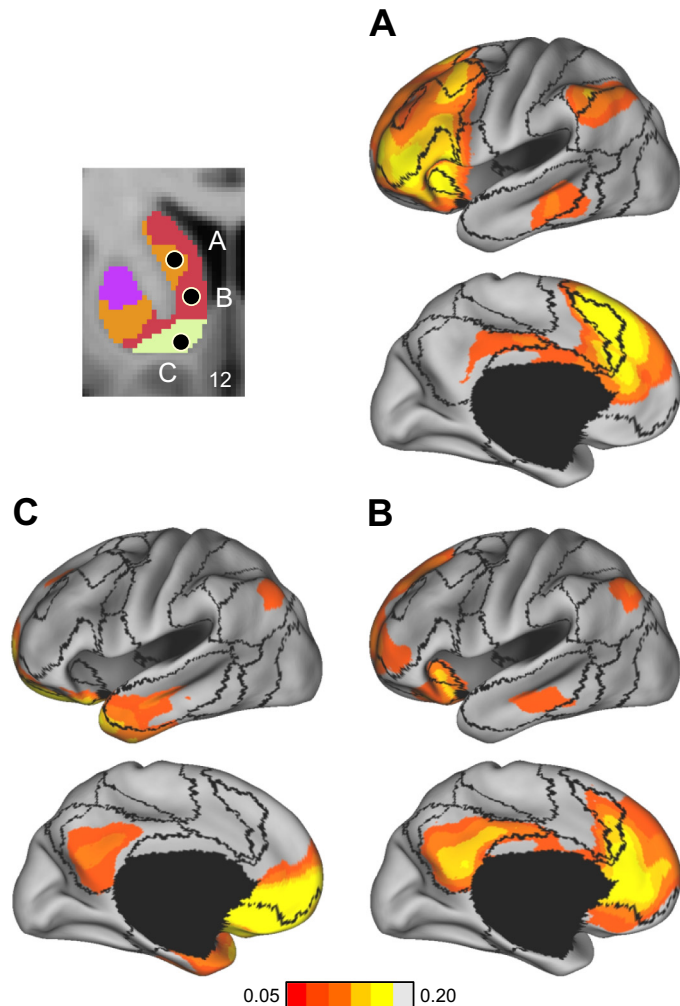
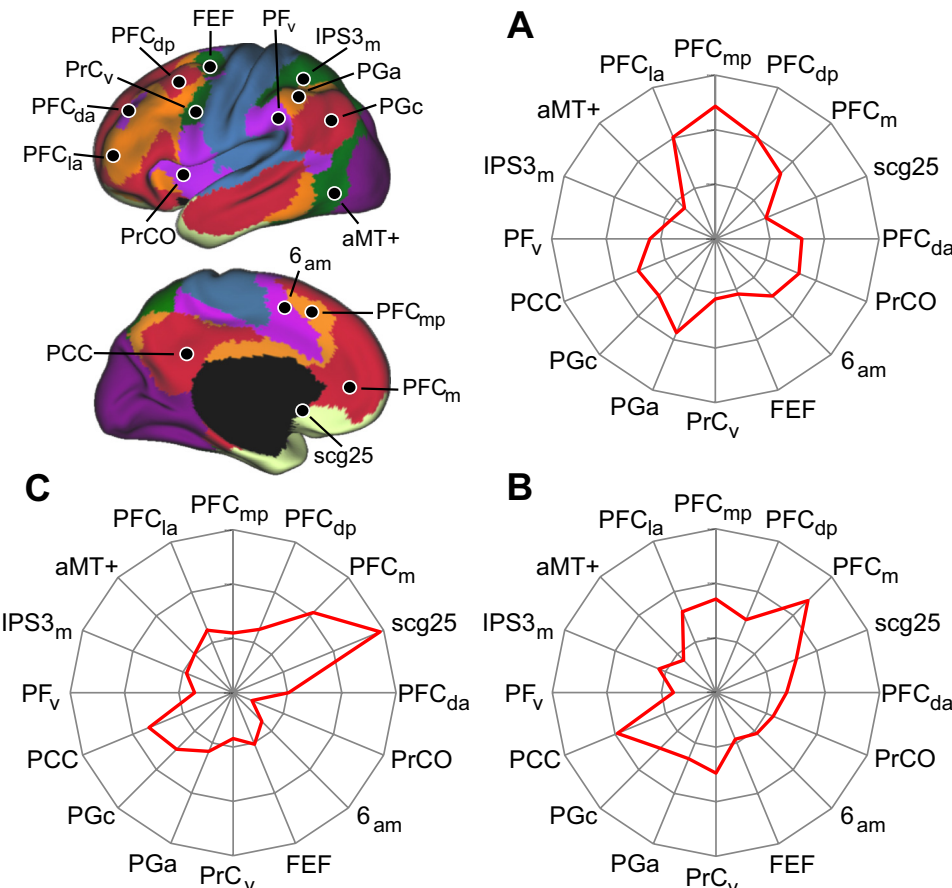


Fig. 11. Evidence for preferential patterns of corticostriatal functional connectivity involving association and limbic networks. Left hemisphere cortical functional connectivity maps derived from the replication sample ( $n = 500$ ) are shown for seed regions placed in high-confidence regions of the striatum from the discovery sample ( $n = 500$ ) for the frontoparietal control (*A*), default (*B*), and limbic (*C*) networks. Seed regions are shown in the center image (Table 2). Separate regions of the striatum are correlated with distinct cerebral networks underlying cognitive and limbic function.

#### *Functional Connectivity of the Striatum in Relation to Monkey Anatomic Connectivity with Association Cortex*

Since the association and limbic networks include cerebral regions that are expanded in humans relative to monkeys (Hill et al. 2010; Van Essen and Dierker 2007), it is difficult to be certain about homologies. There are nonetheless several cases of replicated anatomical projection patterns (at least 2 corroborating injection patterns from 2 independent laboratories) with suspected human homologies (Table 3). Figure 15 shows comparisons for three association and limbic regions, as well as two motor regions as reference. Figure 15*A* shows the seed regions in the dorsolateral prefrontal cortex ( $\text{PFC}_{\text{lp}}$ ), medial prefrontal cortex ( $\text{PFC}_{\text{md}}$ ), and scg25, as well as the motor hand cortex ( $\text{M1}_H$ ) and the SMA from Fig. 5. Figure 15*B* shows representative injection cases from approximately homologous regions in the monkey, while Fig. 15*C* shows human functional connectivity patterns in the replication sample.

The monkey dorsolateral prefrontal cortex injection ( $\text{PFC}_{\text{lp}}$ ) was in the dorsal bank of the principal sulcus and shows a central band of connectivity across the putamen and caudate (Fig. 15, *B*, 3rd column). The corroborating independent observation of this injection pattern is shown in Fig. 16*B* (1st column). This pattern of connectivity in the central band of the putamen and caudate is seen in the corresponding striatal fcMRI map of the dorsolateral prefrontal cortex in the human as well as in the 7-network parcellation, which assigns this region to the frontoparietal control (orange) network. The anatomy for the  $\text{PFC}_{\text{md}}$ , from an injection of area 32, shows a dorsoventral pattern of connectivity that is particularly strong in the medial edge of the caudate (Fig. 15*B*, 4th column). The corroborating independent observation of this medial caudate pattern is seen in the anatomical tracing for  $\text{PFC}_{\text{md}}$  in Fig. 17*B* (4th column). The functional connectivity of the estimated human homolog shows a similar dorsoventral pattern covering the ventral caudate and the dorsal edge of the medial caudate assigned to the default network (red) in the 7-network parcellation. Finally, both the anatomy arising from an area 25 injection in the monkey and the functional connectivity for scg25 showed a pattern covering the nucleus accumbens (Fig. 15*B*, 5th column), which is assigned to the limbic (cream) network in the 7-network parcellation. These selected cases suggest that functional connectivity is capable of identifying association and limbic, as well as motor-related, corticostriatal circuits.



**Fig. 12.** Quantitative evaluation of the specificity of corticostriatal circuits involving association and limbic networks. **A–C:** the 3 polar plots display the functional connectivity correlation values derived from the replication sample ( $n = 500$ ) for each of the striatal seed regions (Table 2) from Fig. 11 with cortical seed regions placed in distributed regions of cortical networks, shown in the center image. Polar scale ranges from  $r = -0.25$  (center) to  $r = 0.35$  (outer boundary) in 0.2-step increments. Each polar plot has a distinct connectivity profile.

#### Functional Connectivity of Association Cortex in Relation to Monkey Anatomy

Previous studies have suggested that anatomically connected cortical areas may project to similar regions of the striatum (Yeterian and Van Hoesen 1978), with complex patterns of overlap and interdigitation (Selemon and Goldman-Rakic 1985). In Figs. 16 and 17, we explored the possible convergence of correlation patterns within the striatum. In Fig. 16 we examined three distributed cortical regions (Fig. 16A) that fell within the frontoparietal control network (orange): PFC<sub>lp</sub>, PGa, and PFC<sub>mp</sub> (Table 3). The fMRI maps of these three cortical regions showed correlations in the dorsal anterior caudate (Fig. 16C), suggesting that functionally related cortical regions are associated with similar regions in the striatum. While there are limitations in comparing tracings between monkeys, anatomic cases in the dorsal bank of the principle sulcus, LIP, and area 9m, respectively, all show projections to the dorsal anterior caudate (Fig. 16B).

In Fig. 17, we compared five cortical regions within the default network (red): the superior temporal sulcus (STS), PGc, PCC, PFC<sub>md</sub>, and PFC<sub>a</sub> (Fig. 17A; Table 3). Injections within putative homologs in the monkey showed a pattern covering the medial edge of the caudate in the anterior half of the striatum for the STS, PFC<sub>md</sub>, and PFC<sub>a</sub> (Fig. 17B), a pattern that was also seen in the functional connectivity in the human (Fig. 17C). Of note, the STS is a region of expansion between the human and the monkey (Hill et al. 2010), which may explain why the region of the human temporal lobe that shows the medial caudate pattern of connectivity does not extend to

the anterior portion of the superior temporal pole, as in the monkey. The functional connectivity maps of the PGc and PCC also showed a medial caudate pattern, but unlike the other regions, the corresponding monkey injection pattern covered only the dorsomedial edge of the caudate. These anatomical patterns were also seen by Yeterian and Pandya (1993) for the PGc and by Powell (1978) for the PCC (see Table 3). We do not understand yet the reasons for this discrepancy. Overall, from these limited cases, these observations support the idea that distributed regions of a functional cortical network are associated with similar regions in the striatum.

#### The Striatum Is Further Divided According to Correlations with More Specific Distributed Cortical Networks

Beyond what can be gleaned from monkey-human comparisons, a detailed analysis of the human striatum reveals a complex organization that may reflect the presence of multiple large-scale circuits. This feature is best illustrated by examining the 17-network parcellation, which generally appears to be a fractionation of the coarser 7-network striatal parcellation. For example, the default network (red) of the 7-network parcellation fractionates into two association networks in the 17-network parcellation. To determine the specificity of this coupling (labeled as red and yellow), we placed seed regions in distributed cortical regions of the two separate association networks in the 17-network model. These consisted of seed regions in the lateral and medial frontal cortex, the PCC, and the parietal cortex (Fig. 18; Table 4). Functional connectivity maps of these seed regions from the replication sample re-

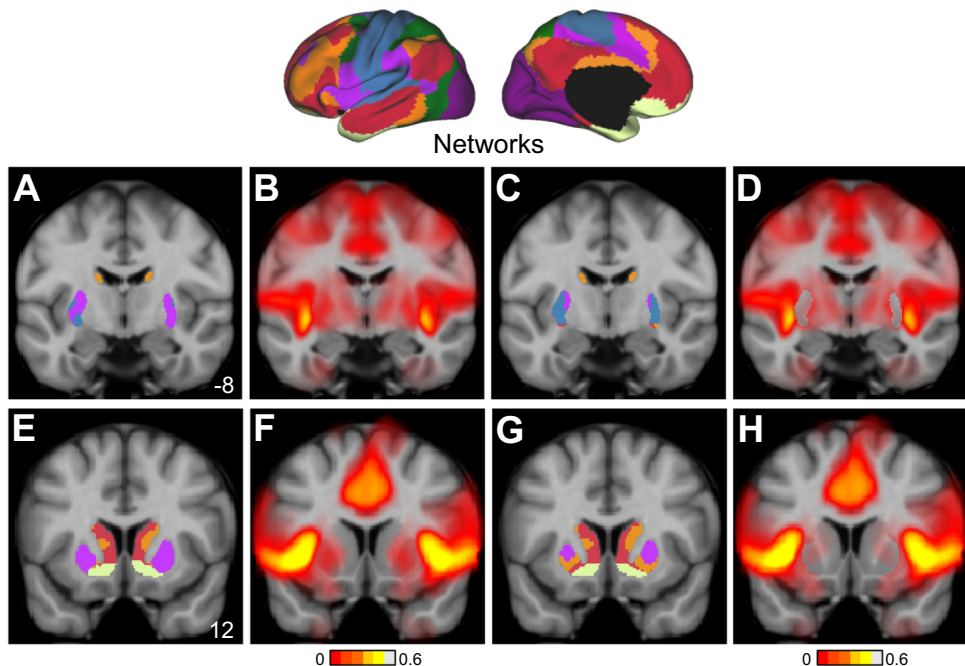


**Fig. 13.** Regression of cortical signal from the striatum. The effects of regressing out the adjacent cortical signal from the striatum are shown with the full sample of 1,000 subjects. *A–D*: posterior striatum ( $y = -8$ ). *E–H*: anterior striatum ( $y = 12$ ). First 2 columns show the 7-network parcellation (*A, E*) and an fcMRI map of a proximal insula seed region (*B, F*) with no cortical signal regression from the striatum (see METHODS for seed region coordinate). Third and fourth columns show the 7-network parcellation (*C, G*) and fcMRI maps of the same seed region (*D, H*) with regression of cortical signal from the striatum (not applied to cortex). Note how the parcellations are dominated by the network labeled by violet. When regression is applied, a more plausible parcellation results. The contrast between the functional connectivity patterns within the striatum before (e.g., *F*) and after (e.g., *H*) regression of adjacent cortical signal illustrates that bleeding of signal from cortex to striatum is mitigated but not fully removed. Signal bleeding minimally affects the major portions of the caudate and ventral striatum. Parcellation estimates within the putamen are less certain.

vealed that the cortical regions in the first association network (red) were preferentially correlated to the dorsal caudate (Fig. 18*A*), while the cortical regions in the second association network (yellow) were preferentially correlated to the ventral caudate (Fig. 18*B*). The specificity of these correlations suggests that subnetworks (e.g., the red and yellow association

networks of the 17-network cortical parcellation) might form distinct circuits with the striatum.

## DISCUSSION

This study characterized the functional organization of the human striatum based on intrinsic functional connectivity to the cerebral cortex. We confirmed the motor zones of the posterior putamen and observed the inverted somatomotor topography in agreement with monkey anatomy. Our results also agree with prior models that divide the striatum into broad functional territories of reward, cognition, and motor function. With the use of detailed analyses of cerebral networks provided by our companion paper (Yeo et al. 2011), we constructed a fine-grained functional map of the complete striatum. Results revealed that the majority of the human striatum's subdivisions are linked to cerebral networks involving distributed regions of association cortex. While gradients dividing striatal zones among reward, cognitive, and motor functions are broadly correct, details of striatal organization present a more complex organization that may parallel the complex interdigitation of large-scale association networks in the cerebral cortex and their projections to overlapping zones within the striatum. In the following sections, we discuss these points in greater detail, as well as caveats and limitations of these striatal parcellation maps.

### The Striatum Is Coupled to Multiple, Distinct Functional Networks in the Cerebral Cortex

Examination of the full striatal parcellation suggested that the striatum is coupled to multiple functional networks within

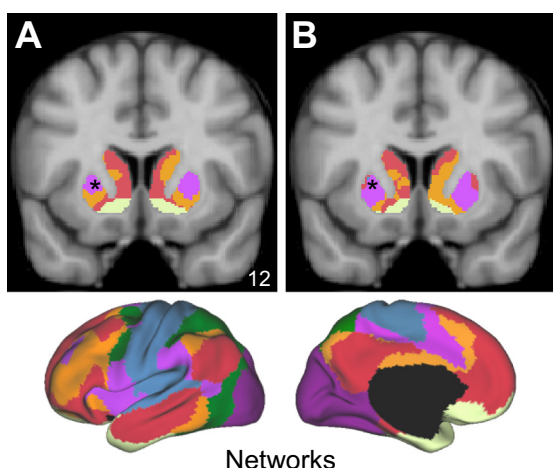


**Fig. 14.** Alternative regression method for removing cortical signal from the striatum. The 7-network parcellation results are shown for the anterior striatum ( $y = 12$ ) using the regression method applied in this paper (*A*; see METHODS and Fig. 13) in which the signal from a unitary cortical mask is regressed from all striatal voxels. An alternative regression method is shown in which for each striatal voxel the signal of neighboring cortical voxels within 9 mm is regressed out (*B*). Asterisk indicates the region of low confidence similar to Fig. 8. The full sample of 1,000 subjects was used.

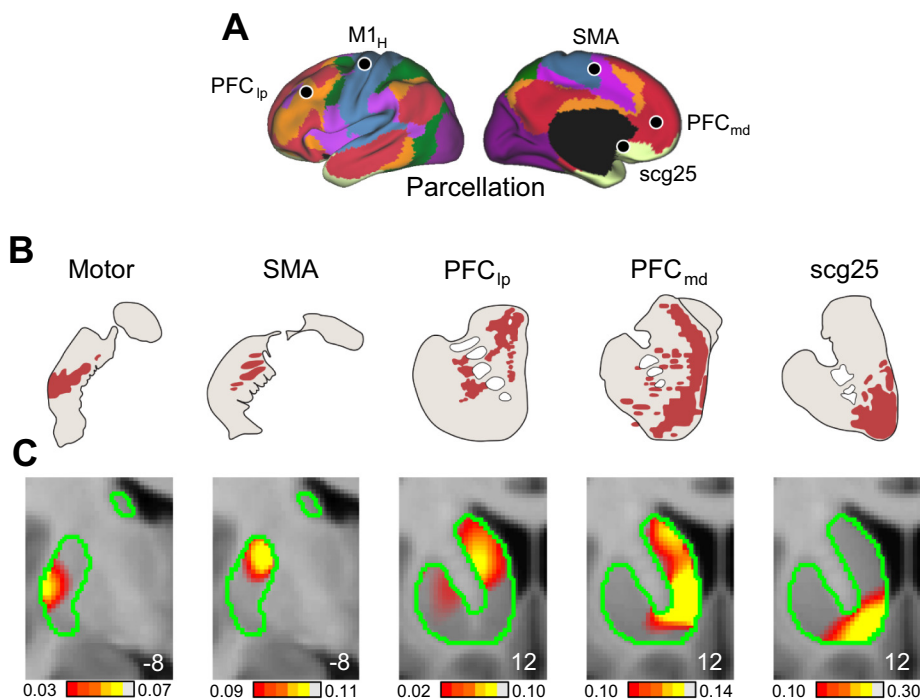


**Fig. 15.** Functional connectivity reveals the distinct topography of motor, association, and limbic networks. *A*: 5 regions with replicated monkey tract-tracings and putative human homologs were selected for comparison: dorsolateral prefrontal cortex (PFC<sub>lp</sub>), medial prefrontal cortex (PFC<sub>md</sub>), estimated subgenual cingulate area 25 (scg25), motor cortex, and SMA. All estimated homologies here and in subsequent figures are uncertain but reasonable approximations based on the available literature. *B*: a representative anatomical tract-tracing case for each region. Cases illustrated are listed in Table 3. *C*: coronal slices show the corresponding functional connectivity generated from the replication sample ( $n = 500$ ) using the seed regions depicted in *A*. Slice atlas coordinates are displayed at bottom right. Note the similarity of the patterns between the anatomy and functional connectivity, as well as their correspondence with the motor (blue), ventral attention (violet), frontoparietal control (orange), default (red), and limbic (cream) parcellations in the 7-network parcellation. Anatomical tract-tracing cases were adapted for conformity as described in Fig. 4 from the following with permission: motor (Liles and Updyke 1985), SMA (Inase et al. 1999), PFC<sub>lp</sub> (Selemon and Goldman-Rakic 1985), scg25 (Haber et al. 2006), and PFC<sub>md</sub> (Ferry et al. 2000). Original tracings from Ferry et al. (2000; PFC<sub>md</sub> and Fig. 17 PFCa) showed the density of axonal synaptic boutons. The redrawing for PFC<sub>md</sub> included only the overlapping circles in the original tracing.

the cerebral cortex. At the broadest level, the parcellation is consistent with models of striatal organization based on monkey tract-tracing studies (Haber et al. 1994; Parent 1990; see also Fig. 15): motor-related subdivisions localized to the posterior putamen (blue in Fig. 7), a limbic-related subdivision localized to the ventral striatum (cream in Fig. 7), and an extensive central band of territory spanning the anterior caudate and putamen linked to association cortex (orange and red in Fig. 7). Tracing studies of the output pathways of the basal ganglia show that they maintain the broad functional segregation of the input pathways to the striatum (Alexander et al. 1986; Middleton and Strick 2002; Strick et al. 1995). Human DTI studies have illustrated a convergent pattern: a dorsal-to-ventral gradient of connections in the anterior striatum from the dorsal PFC to the orbital frontal cortex and an anterior-to-posterior gradient of association to motor cortical connections in the putamen (Bohanna et al. 2011; Cohen et al. 2008; Draganski et al. 2008; Leh et al. 2007; Lehéricy et al. 2004). The present striatal parcellations provide further information with a comprehensive view of the functional architecture of the striatum. For example, the striatal parcellations revealed that the majority of the striatum is dedicated to association cortex (e.g., the frontoparietal control and default network regions). Unlike the motor and ventral attention network zones in the striatum that are localized in the putamen, the striatal association zones span the entire longitudinal extent of the striatum and claim territories in both the caudate and putamen. This

may reflect the limited extent of the motor network versus the parallel, distributed association networks that dominate the human cerebral cortex.

Despite the similarity of the parcellations to the monkey anatomy for motor, limbic, and association networks (Figs. 15–17), there were a few discrepancies for the dorsal attention and visual networks in the 7-network parcellation. The dorsal attention network (green) was present in a region in the right posterior ventral putamen (Fig. 7, coronal slice  $y = -18$  and axial slice  $z = -6$ ). A relaxed striatal mask showed that the posterior caudate was also assigned to the dorsal attention network. These parcellation assignments agree with monkey anatomical projections from the frontal eye field (FEF) and the supplementary eye field (SEF), regions that participate in the dorsal attention network. However, there are also projections from FEF and SEF to the anterior dorsal caudate, often also to the internal capsule and the medial dorsal putamen, which were not seen in the parcellation (Calzavara et al. 2007, Cases 478, 96, and 184; Künzle and Akert 1977, Case 73–228; Parthasarathy et al. 1992, Cases M1, M2, M3, and M5; Stanton et al. 1988, Cases PER, GNA, and TRB; Yeterian and Pandya 1991, Case 9). Examination of correlations from the dorsal attention network revealed that its absence in the parcellation was in part due to striatal correlations that were weaker than other network correlations and thus did not survive the winner-take-all strategy when creating the parcellation. For example, the fMRI map of estimated human FEF showed correlations with the

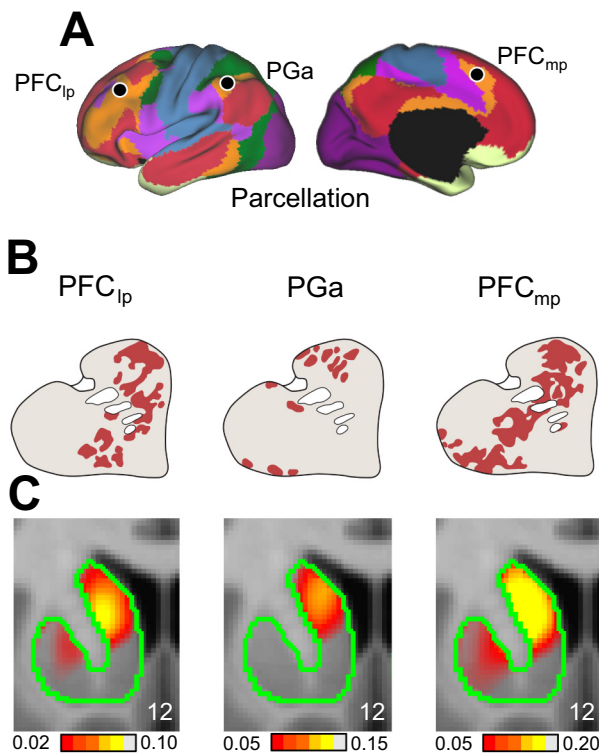


**Fig. 16.** Functional connectivity reveals that distributed cortical regions within the frontoparietal control network couple to similar zones of the striatum. *A*: PFC<sub>ip</sub>, anterior area PG (PGa), and dorsomedial prefrontal cortex (PFC<sub>mp</sub>) were chosen as distributed cortical regions within the frontoparietal control network in order to compare human functional connectivity with monkey anatomy within a single network. *B*: a representative anatomical tract-tracing case for each region. Cases illustrated are listed in Table 3. *C*: coronal slices show the corresponding functional connectivity generated from the replication sample ( $n = 500$ ) using the seed regions depicted in *A*. Slice atlas coordinates are displayed at *bottom right*. Note the broad similarity of the patterns both across the regions and between the monkey anatomy and human functional connectivity. Anatomical tract-tracing cases were adapted as described in Fig. 4 from Selemon and Goldman-Rakic (1985) with permission.

anterior dorsal striatum, which is dominated by correlations from the association networks, but correlations with the posterior ventral putamen were relatively strong enough to be represented in the parcellation.

There was also an absence of the visual network (purple) in the 7-network parcellation. A relaxed striatal mask showed a few voxels assigned to the visual network in primarily bilateral posterior ventral putamen, as well as the anterior-most portion of the head of caudate. Examining the underlying fMRI correlations from striate and extrastriate cortices yielded unexpected results. The fMRI map of V1 showed weak correlations throughout the striatum, while the maps of extrastriate cortex, including from the estimated human MT+ complex, showed virtually no correlation in the striatum (except for weak correlations in the posterior putamen from seed regions in V3 and V4). This is in direct contrast to monkey anatomical tract-tracings that detected corticostriatal projections from extrastriate cortex but not V1 (Maunsell and Van Essen 1983; Saint-Cyr et al. 1990; Ungerleider et al. 1984). The correlations seen from V1 may be due to signal bleeding from correlations in the lateral geniculate nucleus and pulvinar of the thalamus. However, at present, we do not have an explanation for the absence of correlation from extrastriate cortex.

### Distinct Striatal Zones Are Preferentially Coupled to Separate Networks Within Association Cortex

To interpret our results for association cortex, we qualitatively compared the human results to the available tract-tracing studies in the monkey (Table 3). As a heuristic display of correspondence, Fig. 15 shows major zones of the human striatum identified with fMRI compared with examples from reproduced patterns in the monkey literature. Several of these striatal subdivisions linked to association cortex were explored in detail. One caveat to note is that the striatum is characterized by interdigitated projection zones (Selemon and Goldman-Rakic 1985). At the level of our resolution, this overlap may limit what we can reveal with fMRI. Nonetheless, several observed patterns suggested that the majority of the human striatum may be linked to distinct large-scale cerebral association networks and further that distinct zones of the striatum are coupled to the distributed regions that comprise each large-scale network.

**Central caudate head extending into the medial putamen.** One often-observed pattern in the monkey literature arises from tracer injections in the dorsolateral prefrontal cortex. Injections in areas 9 and 46 typically project strongly to the caudate head extending into the medial putamen. The caudate projections continue throughout the body and tail but largely spare the most medial aspects of the caudate (Calzavara et al. 2007; Haber et al. 2006; Selemon and Goldman-Rakic 1985; Yeterian and Pandya 1991). Figure 15 illustrates that a dorsolateral prefrontal seed region (PFC<sub>ip</sub>) couples to a central zone of the human striatum that can be distinguished from the coupling pattern of a medial prefrontal cortex seed region (PFC<sub>mp</sub>) that covers the medial wall of the caudate. The striatal zone coupled to dorsolateral prefrontal region PFC<sub>ip</sub> is associated with the frontoparietal control network (orange network in Fig. 7). The dorsolateral prefrontal cortex has previously been associated with a similar band of territory across the caudate and putamen by DTI (Draganski et al. 2008; Leh et al. 2007; Lehericy et al. 2004) and VBM (Cohen et al. 2008), suggesting that this robust pattern can be observed with multiple techniques.

Of further interest, the striatal zone linked to the frontoparietal control network may receive projections from parietal association cortex. Much like injections of prefrontal areas 9 and 46, injections at or near parietal area 7 include projections through the caudate (Cavada and Goldman-Rakic 1991; Yeterian and Pandya 1993; Yeterian and Van Hoesen 1978). Figure 16 illustrates that cortical association regions distributed throughout the frontoparietal control network, including parietal association cortex (PG<sub>a</sub>), have similar functional coupling patterns in the striatum.

**Medial head of the caudate extending along the medial wall.** In contrast to the central anterior striatum that couples with the frontoparietal control network (Fig. 15; PFC<sub>ip</sub>), the medial wall of the anterior caudate shows specific coupling with the medial prefrontal cortex (Fig. 15; PFC<sub>mp</sub>), a region assigned to the default network in the 7-network parcellation. This pattern was also seen with VBM (Cohen et al. 2008). As with the frontoparietal control network, distributed cortical seed regions within the default network, including parietal region PGc, each show a coupling pattern that involves the medial head of the

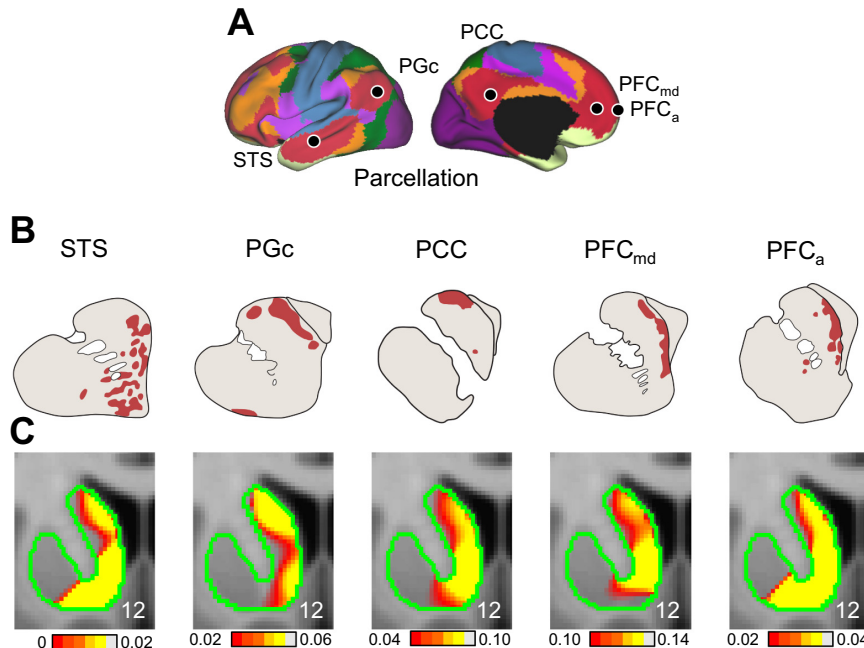


**Fig. 17.** Functional connectivity reveals that distributed cortical regions within the default network couple to similar zones of the striatum. *A:* 5 regions, the superior temporal sulcus (STS), the central portion of area PG (PGc), posterior cingulate cortex (PCC), PFC<sub>md</sub>, and PFC<sub>a</sub> in the frontal pole, with replicated monkey tract-tracings and putative human homologs were selected to compare functional connectivity with monkey anatomy within the default network (red). Cases illustrated are adapted from cases in Table 3. *B:* a representative anatomical tract-tracing case for each region. *C:* coronal slices show the corresponding functional connectivity generated from the replication sample ( $n = 500$ ) using the seed regions depicted in *A*. Slice atlas coordinates are displayed at bottom right. Note the general similarity of the patterns both across the regions and between the monkey anatomy and human functional connectivity. However, several discrepancies are also notable including the differences between PGc and PCC and STS. Anatomical tract-tracing cases were adapted as described in Figs. 4 and 15 from the following with permission: STS (Selemon and Goldman-Rakic 1985), PGc (Cavada and Goldman-Rakic 1991), PCC (Baleydier and Mauguire 1980), and PFC<sub>md</sub> (Yeterian and Pandya 1991) and PFC<sub>a</sub> (Ferry et al. 2000).

caudate, in most cases along the dorsoventral extent of the medial wall (Fig. 17).

**Neighboring striatal zones couple to different association networks.** In addition to the single-injection case studies presented in Figs. 15–17 illustrating the coupling of striatal zones to distributed cortical networks, several studies have examined differing corticostriatal projection patterns in adjacent striatal zones. Through a series of double-labeling cases, Selemon and Goldman-Rakic (1985) showed that dorsolateral prefrontal cortical projections terminate in the central portion of the caudate head extending into the medial putamen (their Case 16; highly similar to case PFC<sub>lp</sub> illustrated in the present Fig. 16). By contrast, orbital frontal projections terminated along the medial wall in a pattern more similar to those observed for the medial prefrontal injections illustrated in Fig. 17 (PFC<sub>md</sub> and PFC<sub>a</sub>). Thus the medial head of the caudate is linked more with medial and orbital frontal regions than are the central zones of the caudate. All of these projections extend through the anterior-to-posterior axis of the striatum with the medial-to-lateral pattern best visualized in the head of the caudate.

Cavada and Goldman-Rakic (1991) further report a telling set of tracing injections that contrast 7a/Opt with 7ip within parietal association cortex. An injection at or near 7a/Opt displayed overlapping but medially located projections to those from 7ip in the dorsal caudate head, paralleling the human parcellation boundary between the default network and the frontoparietal control network. We suspect that the injections of 7a/Opt fall within the monkey homolog of the default network: the posterior portion of 7a that comprises Opt in the monkey is connected to the parahippocampal gyrus and posterior cingulate, and minimally so with distant sensory and motor regions (see, e.g., Andersen et al. 1990, Case 5; Barnes and Pandya 1992, Cases 1 and 2; Cavada and Goldman-Rakic 1989, Case 2; Mesulam et al. 1977, Case 1). However, while the 7a/Opt projections to the striatum fall medial to those arising from 7ip, they do not extend down the medial wall (e.g., also see Yeterian and Pandya 1993, Case 22) as seen from injections in other posteriorly located (putative) homologs of

the default network in monkeys (Fig. 17; PGc and PCC). Nonetheless, there is a medial-to-lateral gradient for parietal regions that, like prefrontal cortex, roughly divides the anterior caudate between the estimated anatomy of the default network and frontoparietal control network.

This medial-to-lateral distinction divides the striatum based on large-scale networks that each possess prefrontal and parietal components. Selemon and Goldman-Rakic (1985, their Fig. 15) suggested that projections from the posterior parietal cortex and dorsolateral prefrontal cortex are located preferentially in separate regions of the striatum. Despite the apparent discrepancy with our data, it is possible that these two models of organization are consistent if one considers the overlap between the posterior parietal and dorsolateral prefrontal projections (Selemon and Goldman-Rakic 1985, their Fig. 9) and the possibility that these injections cover different association networks, each with their distinct striatal projection zones.

**Striatal zones distinguish juxtaposed cerebral association networks.** The above discussion highlights evidence that distinct large-scale networks of association cortex are coupled to adjacent but distinct zones of the striatum. This principle can be further extended. With the fine-parcellated segmentation of the cerebral cortex as a guide, distributed regions that fall within anatomically adjacent (but functionally distinct) networks were shown to have subtly different coupling patterns in the striatum. Figure 18 displays an example. Two sets of regions are plotted that each fall within a separate distributed large-scale association network. While these two sets of regions show overlapping functional coupling patterns within the striatum, a consistent difference emerges, with one network preferentially coupled to the dorsal medial head of the caudate (Fig. 18A) and the second network preferentially coupled to the ventral medial head of the caudate (Fig. 18B). This difference in preferential coupling extends to the juxtaposed parietal regions PG<sub>a</sub> and PG<sub>dp</sub>. It is also of interest that the regions of the default network most closely associated with limbic structures (PCC, PFC<sub>m</sub>, and PG<sub>dp</sub>) are linked to striatal zones that fall between the nucleus accumbens and striatal zones

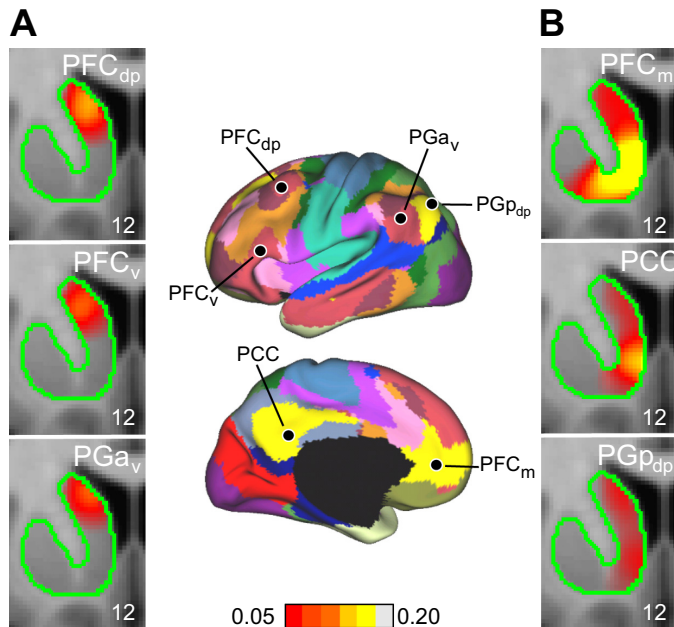


**Fig. 18.** Functional connectivity reveals that interdigitated cerebral association networks couple to nearby but preferentially distinct zones of the striatum. Two association networks that each comprise distributed regions within the cortex (labeled red and yellow) in the 17-network parcellation were selected to examine fine-grained features of corticostriatal organization. *Center:* 3 seed regions distributed across the brain for each network (Table 4). Seed regions were obtained from Yeo et al. (2011) except for ventral anterior area PG ( $PG_{av}$ ) and the dorsal posterior portion of posterior area PG ( $PGp_{dp}$ ). Functional connectivity was computed with the replication sample ( $n = 500$ ). *A:* the functional connectivity of  $PFC_{dp}$ ,  $PFC_v$ , and  $PGa_v$  from the red association network converge on similar zones of dorsal caudate head (shown in coronal slice  $y = 12$ ). *B:* by contrast, the functional connectivity of  $PGp_{dp}$ ,  $PCC$ , and  $PFC_m$  from the yellow association network converge upon similar zones of the ventral caudate head. Note that spatially juxtaposed cerebral regions (e.g.,  $PGa_v$  and  $PGp_{dp}$ ) coupled to distinct striatal zones consistent with their belonging to separate large-scale cerebral networks.

linked to the dorsolateral prefrontal cortex (the central caudate head). These findings reinforce the idea that distinct large-scale networks, which comprise the majority of the human cerebral mantle, are coupled to distinct zones of the striatum. Moreover, the widely distributed regions within each cerebral network show similar functional coupling within the striatum.

#### Basis of Striatal Coupling to Distributed Cerebral Regions

Evidence from studies examining retrograde tracer injections in the striatum anticipates the results we illustrate in the human. Arikuni and Kubota (1986) showed that retrograde injections into the ventromedial caudate of the monkey striatum lead to tracer uptake distributed in the OFC, lateral frontal lobe, and temporal lobe (parietal and medial frontal cortices were not reported). In the cat, Rosell and Gimenez-Amaya (1999) showed that retrograde injections in the dorsal anterior caudate result in labeled neurons in distributed frontal, parietal, and temporal cortices. In a comprehensive set of tracings in the rat, McGeorge and Faull (1989) showed that retrograde injections in the striatum lead to tracer uptake in distributed regions of the neocortex, mesocortex, and allocortex. We show here in humans that functional connectivity from a single striatal seed region produces a distributed pattern of cortical correlations (Fig. 11). DTI studies have also shown that seed regions of the striatum have distributed connections with the cerebral cortex

(Draganski et al. 2008; Leh et al. 2007). These combined observations suggest that the striatum is functionally integrated with distributed cortical networks. We cannot, however, observe the microstructural organization and connectivity of these correlations.

Previous studies in the monkey shed insight into the details of convergent projection patterns in the striatum. Yeterian and Van Hoesen (1978) proposed that cortical regions connected to one another share projection zones in the striatum. Selemon and Goldman-Rakic (1985) refined this observation, using double-labeled cases. In their seminal study, they revealed that projections from parietal and frontal cortex only partially overlapped, and when overlap was present an interdigitated pattern emerged, suggesting that projections between prefrontal and parietal regions do not commonly project to the same striatal neurons. The present results cannot resolve this level of anatomic detail, but the consistent and robust functional coupling patterns observed between distributed cortical regions and common striatal zones raises again the possibility that striatal zones may in some way integrate connections from widely distributed cortical regions. Our results provide a clue that may help us understand prior results. As illustrated in Fig. 18, nearby cerebral regions can participate in distinct cerebral networks and couple to separate striatal zones. The adjacency of these cortical networks and their striatal targets may partially explain the limited overlap observed by Selemon and Goldman-Rakic in their double-labeled cases. Although these injections were confirmed to be in anatomically connected cortical regions, they each tended to cover a large territory that might include multiple areas with diverse connectivity profiles. Thus partial overlap in the striatum may result when the injections into frontal and parietal regions sample distinct combinations of cerebral networks.

#### Caveats and Limitations

It is important to note that measuring functional connectivity is not the same as measuring anatomic connectivity, thus limiting the conclusions that can be drawn from our work (previously discussed in Buckner et al. 2011; Yeo et al. 2011). Limitations include the inability to determine the directionality of the connectivity and to interpret our striatal parcellations as rigid representations of anatomic connectivity. It is intriguing how well human striatal functional connectivity corresponds to gross topographic patterns from monkey anatomic tracings.

**Table 4.** Locations of seed regions used for functional connectivity of distributed cortical networks

Cerebral Cortex	Left Hemi Coordinates
PCC	-3, -49, 25
$PFC_m$	-7, 46, -2
$PFC_{dp}$	-44, 15, 48
$PFC_v$	-55, 24, 13
$PGa_v$	-54, -54, 35
$PGp_{dp}$	-43, -70, 43

Left hemisphere cerebral cortical seed regions were obtained from Yeo et al. (2011) except for anterior ventral area PG ( $PG_{av}$ ) and the dorsal posterior portion of posterior area PG ( $PGp_{dp}$ ), which were selected from the cortical regions in the yellow association network in the 17-network parcellation of the discovery data set. They were named based on probabilistic histological maps of nearby areas (Caspers et al. 2006; Geyer 2004).

Nonetheless, we feel confident that there will be discrepancies and boundary conditions to this correspondence because functional connectivity is constrained but not fully dictated by anatomic connectivity.

A major limitation of the present work is resolution, which prevents the observation of striatal microstructure, including the overlap or interdigitation of connections in striosomes and matrisomes. In addition, in a structure with observed interdigitation of projections, our winner-take-all strategy may be misleading in regions with a high heterogeneity of connections. For these reasons, we recommend viewing the parcellations with the aid of the confidence maps, as well as examining the underlying functional connectivity for any particular region of interest. The strength of these parcellation maps is that they give a comprehensive view of the functional territories of the striatum; however, their utility is limited for certain questions.

Resolution also impacted our results in a way that is particularly problematic for the striatum. The striatum is near to the cerebral cortex, in particular the putamen and the insula, resulting in signal bleeding across the cortical-striatal boundary that can be partially, but not entirely, mitigated (Figs. 13 and 14). We suspect that the pink network assignment in the anterior putamen of the 17-network parcellation (Fig. 8) is a result of signal bleeding from the adjacent insula. For this reason, we are least confident about the details of our parcellations around the dorsal putamen. High-resolution functional imaging (e.g., ~1 mm) in individual subjects at high field may circumvent this issue in future studies.

A further limitation of our work is that we only mapped the striatal coupling to the cerebral cortex. There are strong projections to the striatum from subcortical structures, which we have not considered here, such as the amygdala (Fudge et al. 2002, 2004; Russchen et al. 1985) and the cerebellum via the thalamus (Hoshi et al. 2005). We refer interested readers to another study examining the functional connectivity of the amygdala to the striatum (Roy et al. 2009).

### Conclusions

Specific striatal zones are functionally coupled to distinct cerebral networks. As seen by prior studies, the posterior putamen is dedicated to motor function and the nucleus accumbens to limbic function. The remaining majority of the striatum is connected to parallel, distributed association networks that may underlie contributions of the striatum to higher cognitive functions.

### ACKNOWLEDGMENTS

We thank Fenna Krienen and Avram Holmes for discussion, Koene Van Dijk for helpful comments on the manuscript, the Harvard Center for Brain Science Neuroimaging Core and the Athinoula A. Martinos Center for imaging support, the Harvard FAS Research Computing Group (in particular James Cuff, Brian Mantenuo, and Luis Silva), and the Harvard Neuroinformatics Research Group (Gabriele Fariello, Timothy O'Keefe, and Victor Petrov). We thank Haderer & Müller Biomedical Art for anatomic illustrations. E. Y. Choi was supported by fellowships from the Advanced Multimodal Neuroimaging Training Program and the National Science Foundation.

### GRANTS

This work was supported by National Institutes of Health (NIH) Grants AG-021910, A6-034556, P41-RR-14074, and K08-MH-067966, the Massachusetts General Hospital-University of California, Los Angeles Human Con-

nectome Project (U54MH091665), the Howard Hughes Medical Institute, and the Simons Foundation. The content is solely the responsibility of the authors and does not necessarily represent the official views of NIH.

### DISCLOSURES

R. L. Buckner is a consultant for Pfizer, Inc.

### AUTHOR CONTRIBUTIONS

Author contributions: E.Y.C., B.T.Y., and R.L.B. conception and design of research; E.Y.C. and B.T.Y. performed experiments; E.Y.C. and B.T.Y. analyzed data; E.Y.C., B.T.Y., and R.L.B. interpreted results of experiments; E.Y.C. prepared figures; E.Y.C. drafted manuscript; E.Y.C., B.T.Y., and R.L.B. edited and revised manuscript; R.L.B. approved final version of manuscript.

### REFERENCES

- Alexander GE, Crutcher MD, DeLong MR.** Basal ganglia-thalamocortical circuits: parallel substrates for motor, oculomotor, "prefrontal" and "limbic" functions. *Prog Brain Res* 85: 119–146, 1990.
- Alexander GE, DeLong MR.** Microstimulation of the primate neostriatum. II. Somatotopic organization of striatal microexcitable zones and their relation to neuronal response properties. *J Neurophysiol* 53: 1417–1430, 1985.
- Alexander GE, DeLong MR, Strick PL.** Parallel organization of functionally segregated circuits linking basal ganglia and cortex. *Annu Rev Neurosci* 9: 357–381, 1986.
- Andersen RA, Asanuma C, Essick G, Siegel RM.** Corticocortical connections of anatomically and physiologically defined subdivisions within the inferior parietal lobule. *J Comp Neurol* 296: 65–113, 1990.
- Arikuni T, Kubota K.** The organization of prefrontocaudate projections and their laminar origin in the macaque monkey: a retrograde study using HRP-gel. *J Comp Neurol* 244: 492–510, 1986.
- Baleydier C, Mauguire F.** The duality of the cingulate gyrus in monkey. Neuroanatomical study and functional hypothesis. *Brain* 103: 525–554, 1980.
- Barnes CL, Pandya DN.** Efferent cortical connections of multimodal cortex of the superior temporal sulcus in the rhesus monkey. *J Comp Neurol* 318: 222–244, 1992.
- Barnes KA, Cohen AL, Power JD, Nelson SM, Dosenbach YB, Miezin FM, Petersen SE, Schlaggar BL.** Identifying basal ganglia divisions in individuals using resting-state functional connectivity MRI. *Front Syst Neurosci* 4: 18, 2010.
- Biswal B, Yetkin FZ, Haughton VM, Hyde JS.** Functional connectivity in the motor cortex of resting human brain using echo-planar MRI. *Magn Reson Med* 34: 537–541, 1995.
- Biswal BB, Mennes M, Zuo XN, Gohel S, Kelly C, Smith SM, Beckmann CF, Adelstein JS, Buckner RL, Colcombe S, Dogonowski AM, Ernst M, Fair D, Hampson M, Hoptman MJ, Hyde JS, Kiviniemi VJ, Kotter R, Li SJ, Lin CP, Lowe MJ, Mackay C, Madden DJ, Madsen KH, Margulies DS, Mayberg HS, McMahon K, Monk CS, Mostofsky SH, Nagel BJ, Pekar JJ, Peltier SJ, Petersen SE, Riedl V, Rombouts SA, Rypma B, Schlaggar BL, Schmidt S, Seidler RD, Siegle GJ, Sorg C, Teng GJ, Veijola J, Villringer A, Walter M, Wang L, Weng XC, Whitfield-Gabrieli S, Williamson P, Windischberger C, Zang YF, Zhang HY, Castellanos FX, Milham MP.** Toward discovery science of human brain function. *Proc Natl Acad Sci USA* 107: 4734–4739, 2010.
- Boahna I, Georgiou-Karistianis N, Egan GF.** Connectivity-based segmentation of the striatum in Huntington's disease: vulnerability of motor pathways. *Neurobiol Dis* 42: 475–481, 2011.
- Brett M.** *The MNI Brain and the Talairach Atlas* (Online). <http://imaging.mrc-cbu.cam.ac.uk/imaging/MniTalairach>.
- Buckner RL.** Human functional connectivity: new tools, unresolved questions. *Proc Natl Acad Sci USA* 107: 10769–10770, 2010.
- Buckner RL, Andrews-Hanna JR, Schacter DL.** The brain's default network: anatomy, function, and relevance to disease. *Ann NY Acad Sci* 1124: 1–38, 2008.
- Buckner RL, Krienen FM, Castellanos A, Diaz JC, Yeo BT.** The organization of the human cerebellum estimated by intrinsic functional connectivity. *J Neurophysiol* 106: 2322–2345, 2011.
- Calzavarra R, Mailly P, Haber SN.** Relationship between the corticostriatal terminals from areas 9 and 46, and those from area 8A, dorsal and rostral

- premotor cortex and area 24c: an anatomical substrate for cognition to action. *Eur J Neurosci* 26: 2005–2024, 2007.
- Caspers S, Geyer S, Schleicher A, Mohlberg H, Amunts K, Zilles K.** The human inferior parietal cortex: cytoarchitectonic parcellation and interindividual variability. *Neuroimage* 33: 430–448, 2006.
- Cavada C, Goldman-Rakic PS.** Posterior parietal cortex in rhesus monkey. I. Parcellation of areas based on distinctive limbic and sensory corticocortical connections. *J Comp Neurol* 287: 393–421, 1989.
- Cavada C, Goldman-Rakic PS.** Topographic segregation of corticostratial projections from posterior parietal subdivisions in the macaque monkey. *Neuroscience* 42: 683–696, 1991.
- Cohen MX, Lombardo MV, Blumenfeld RS.** Covariance-based subdivision of the human striatum using T1-weighted MRI. *Eur J Neurosci* 27: 1534–1546, 2008.
- Dale AM, Fischl B, Sereno MI.** Cortical surface-based analysis. I. Segmentation and surface reconstruction. *Neuroimage* 9: 179–194, 1999.
- DeLong MR, Georgopoulos AP.** Motor functions of the basal ganglia. In: *Handbook of Physiology. The Nervous System. Motor Control*. Bethesda, MD: Am Physiol Soc, 1981, sect. 1, vol. II, part 2, p. 1017–1061.
- Di Martino A, Scheres A, Margulies DS, Kelly AM, Uddin LQ, Shehzad Z, Biswal B, Walters JR, Castellanos FX, Milham MP.** Functional connectivity of human striatum: a resting state fMRI study. *Cereb Cortex* 18: 2735–2747, 2008.
- Draganski B, Kherif F, Klöppel S, Cook PA, Alexander DC, Parker GJ, Deichmann R, Ashburner J, Frackowiak RS.** Evidence for segregated and integrative connectivity patterns in the human basal ganglia. *J Neurosci* 28: 7143–7152, 2008.
- Eblen F, Graybiel AM.** Highly restricted origin of prefrontal cortical inputs to striosomes in the macaque monkey. *J Neurosci* 15: 5999–6013, 1995.
- Evans AC, Collins DL, Mills SR, Brown ED, Kelly RL, Peters TM.** 3D statistical neuroanatomical models from 305 MRI volumes. In: *Proceedings of IEEE Nuclear Science Symposium and Medical Imaging Conference*. London: MTP, 1993, vol. 95, p. 1813–1817.
- Ferry AT, Öngür D, An X, Price JL.** Prefrontal cortical projections to the striatum in macaque monkeys: evidence for an organization related to prefrontal networks. *J Comp Neurol* 425: 447–470, 2000.
- Fischl B, Liu A, Dale AM.** Automated manifold surgery: constructing geometrically accurate and topologically correct models of the human cerebral cortex. *IEEE Trans Med Imaging* 20: 70–80, 2001.
- Fischl B, Rajendran N, Busa E, Augustinack J, Hinds O, Yeo BT, Mohlberg H, Amunts K, Zilles K.** Cortical folding patterns and predicting cytoarchitecture. *Cereb Cortex* 18: 1973–1980, 2008.
- Fischl B, Salat DH, Busa E, Albert M, Dieterich M, Haselgrove C, van der Kouwe A, Killiany R, Kennedy D, Klaveness S, Montillo A, Makris N, Rosen B, Dale AM.** Whole brain segmentation: automated labeling of neuroanatomical structures in the human brain. *Neuron* 33: 341–355, 2002.
- Fischl B, Sereno MI, Dale AM.** Cortical surface-based analysis. II. Inflation, flattening, and a surface-based coordinate system. *Neuroimage* 9: 195–207, 1999a.
- Fischl B, Sereno MI, Tootell RB, Dale AM.** High-resolution intersubject averaging and a coordinate system for the cortical surface. *Hum Brain Mapp* 8: 272–284, 1999b.
- Fischl B, Salat DH, van der Kouwe AJ, Makris N, Ségonne F, Quinn BT, Dale AM.** Sequence-independent segmentation of magnetic resonance images. *Neuroimage* 23: S69–S84, 2004.
- Fitzgerald PB, Laird AR, Maller J, Daskalakis ZJ.** A meta-analytic study of changes in brain activation in depression. *Hum Brain Mapp* 29: 683–695, 2008.
- Flaherty AW, Graybiel AM.** Two input systems for body representations in the primate striatal matrix: experimental evidence in the squirrel monkey. *J Neurosci* 13: 1120–1137, 1993.
- Flaherty AW, Graybiel AM.** Input-output organization of the sensorimotor striatum in the squirrel monkey. *J Neurosci* 14: 599–610, 1994.
- Fonov V, Evans AC, Botteron K, Almlie CR, McKinstry RC, Collins DL, Brain Development Cooperative Group.** Unbiased average age-appropriate atlases for pediatric studies. *Neuroimage* 54: 313–327, 2011.
- Fornito A, Bullmore ET.** What can spontaneous fluctuations of the blood oxygenation-level-dependent signal tell us about psychiatric disorders? *Curr Opin Psychiatry* 23: 239–249, 2010.
- Fox MD, Raichle ME.** Spontaneous fluctuations in brain activity observed with functional magnetic resonance imaging. *Nat Rev Neurosci* 8: 700–711, 2007.
- Fudge JL, Breitbart MA, McClain C.** Amygdaloid inputs define a caudal component of the ventral striatum in primates. *J Comp Neurol* 476: 330–347, 2004.
- Fudge JL, Kunishio K, Walsh P, Richard C, Haber SN.** Amygdaloid projections to ventromedial striatal subterritories in the primate. *Neuroscience* 110: 257–275, 2002.
- Geyer S.** The microstructural border between the motor and the cognitive domain in the human cerebral cortex. *Adv Anat Embryol Cell Biol* 174: 1–89, 2004.
- Geyer S, Ledberg A, Schleicher A, Kinomura S, Schormann T, Burgel U, Klingberg T, Larsson J, Zilles K, Roland PE.** Two different areas within the primary motor cortex of man. *Nature* 382: 805–807, 1996.
- Grefkes C, Geyer S, Schormann T, Roland P, Zilles K.** Human somatosensory area 2: observer-independent cytoarchitectonic mapping, interindividual variability, and population map. *Neuroimage* 14: 617–631, 2001.
- Greve DN, Fischl B.** Accurate and robust brain image alignment using boundary-based registration. *Neuroimage* 48: 63–72, 2009.
- Haber SN.** The primate basal ganglia: parallel and integrative networks. *J Chem Neuroanat* 26: 317–330, 2003.
- Haber SN, Gdowski MJ.** The basal ganglia. In: *The Human Nervous System* (2nd ed.), edited by Paxinos G, Mai JK. Amsterdam: Elsevier Academic, 2004.
- Haber SN, Kim KS, Mailly P, Calzavara R.** Reward-related cortical inputs define a large striatal region in primates that interface with associative cortical connections, providing a substrate for incentive-based learning. *J Neurosci* 26: 8368–8376, 2006.
- Haber SN, Lynd-Balta E, Spooren WP.** Integrative aspects of basal ganglia circuitry. In: *Basal Ganglia IV*, edited by Percheron G, McKenzie JS, Féger J. New York: Plenum, 1994.
- Hill J, Inder T, Neil J, Dierker D, Harwell J, Van Essen D.** Similar patterns of cortical expansion during human development and evolution. *Proc Natl Acad Sci USA* 107: 13135–13140, 2010.
- Hoshi E, Tremblay L, Féger J, Carras PL, Strick PL.** The cerebellum communicates with the basal ganglia. *Nat Neurosci* 8: 1491–1493, 2005.
- Inase M, Sakai ST, Tanji J.** Overlapping corticostratial projections from the supplementary motor area and the primary motor cortex in the macaque monkey: an anterograde double labeling study. *J Comp Neurol* 373: 283–296, 1996.
- Inase M, Tokuno H, Nambu A, Akazawa T, Takada M.** Corticostratial and corticosubthalamic input zones from the presupplementary motor area in the macaque monkey: comparison with the input zones from the supplementary motor area. *Brain Res* 833: 191–201, 1999.
- Jenkinson M, Bannister P, Brady M, Smith S.** Improved optimization for the robust and accurate linear registration and motion correction of brain images. *Neuroimage* 17: 825–841, 2002.
- Künzle H.** Bilateral projections from precentral motor cortex to the putamen and other parts of the basal ganglia. An autoradiographic study in *Macaca fascicularis*. *Brain Res* 88: 195–209, 1975.
- Künzle H, Akert K.** Efferent connections of cortical, area 8 (frontal eye field) in *Macaca fascicularis*. A reinvestigation using the autoradiographic technique. *J Comp Neurol* 173: 147–164, 1977.
- Kwong KK, Belliveau JW, Chesler DA, Goldberg IE, Weisskoff RM, Poncelet BP, Kennedy DN, Hoppel BE, Cohen MS, Turner R, Cheng HM, Brady TJ, Rosen BR.** Dynamic magnetic resonance imaging of human brain activity during primary sensory stimulation. *Proc Natl Acad Sci USA* 89: 5675–5679, 1992.
- Leh SE, Ptito A, Chakravarty MM, Strafella AP.** Fronto-striatal connections in the human brain: a probabilistic diffusion tractography study. *Neurosci Lett* 419: 113–118, 2007.
- Lehéricy S, Ducros M, Van de Moortele PF, Francois C, Thivard L, Poupon C, Swindale N, Ugurbil K, Kim DS.** Diffusion tensor fiber tracking shows distinct corticostratial circuits in humans. *Ann Neurol* 55: 522–529, 2004.
- Liles SL, Updyke BV.** Projection of the digit and wrist area of precentral gyrus to the putamen: relation between topography and physiological properties of neurons in the putamen. *Brain Res* 339: 245–255, 1985.
- MacLean PD.** Cerebral evolution and emotional processes: new findings on the striatal complex. *Ann NY Acad Sci* 193: 137–149, 1972.
- Marcus DS, Fotenos AF, Csernansky JG, Morris JC, Buckner RL.** Open access series of imaging studies: longitudinal MRI data in nondemented and demented older adults. *J Cogn Neurosci* 22: 2677–2684, 2010.
- Marcus DS, Wang TH, Parker J, Csernansky JG, Morris JC, Buckner RL.** Open Access Series of Imaging Studies (OASIS): cross-sectional MRI

- data in young, middle aged, nondemented, and demented older adults. *J Cogn Neurosci* 19: 1498–1507, 2007.
- Maunsell JH, Van Essen DC.** The connections of the middle temporal visual area (MT) and their relationship to a cortical hierarchy in the macaque monkey. *J Neurosci* 3: 2563–2586, 1983.
- McGeorge AJ, Faull RL.** The organization of the projection from the cerebral cortex to the striatum in the rat. *Neuroscience* 29: 503–537, 1989.
- Mesulam MM, Van Hoesen GW, Pandya DN, Geschwind N.** Limbic and sensory connections of the inferior parietal lobule (area PG) in the rhesus monkey: a study with a new method for horseradish peroxidase histochemistry. *Brain Res* 136: 393–414, 1977.
- Middleton FA, Strick PL.** Basal-ganglia “projections” to the prefrontal cortex of the primate. *Cereb Cortex* 12: 926–935, 2002.
- Ogawa S, Tank DW, Menon R, Ellermann JM, Kim SG, Merkle H, Ugurbil K.** Intrinsic signal changes accompanying sensory stimulation: functional brain mapping with magnetic resonance imaging. *Proc Natl Acad Sci USA* 89: 5951–5955, 1992.
- Öngür D, Ferry AT, Price JL.** Architectonic subdivision of the human orbital and medial prefrontal cortex. *J Comp Neurol* 460: 425–449, 2003.
- Parent A.** Extrinsic connections of the basal ganglia. *Trends Neurosci* 13: 254–258, 1990.
- Parent A, Hazrati LN.** Functional anatomy of the basal ganglia. I. The cortico-basal ganglia-thalamo-cortical loop. *Brain Res Rev* 20: 91–127, 1995.
- Parthasarathy HB, Schall JD, Graybiel AM.** Distributed but convergent ordering of corticostriatal projections: analysis of the frontal eye field and the supplementary eye field in the macaque monkey. *J Neurosci* 12: 4468–4488, 1992.
- Petrides M, Pandya DN.** Dorsolateral prefrontal cortex: comparative cytoarchitectonic analysis in the human and the macaque brain and corticocortical connection patterns. *Eur J Neurosci* 11: 1011–1036, 1999.
- Picard N, Strick PL.** Motor areas of the medial wall: a review of their location and functional activation. *Cereb Cortex* 6: 342–353, 1996.
- Postuma RB, Dagher A.** Basal ganglia functional connectivity based on a meta-analysis of 126 positron emission tomography and functional magnetic resonance imaging publications. *Cereb Cortex* 16: 1508–1521, 2006.
- Powell EW.** The cingulate bridge between allocortex, isocortex and thalamus. *Anat Rec* 190: 783–793, 1978.
- Power JD, Cohen AL, Nelson SM, Wig GS, Barnes KA, Church JA, Vogel AC, Laumann TO, Miezin FM, Schlaggar BL, Petersen SE.** Functional network organization of the human brain. *Neuron* 72: 665–678, 2011.
- Power JD, Fair DA, Schlaggar BL, Petersen SE.** The development of human functional brain networks. *Neuron* 67: 735–748, 2010.
- Rosell A, Gimenez-Amaya JM.** Anatomical re-evaluation of the corticostriatal projections to the caudate nucleus: a retrograde labeling study in the cat. *Neurosci Res* 34: 257–269, 1999.
- Roy AK, Shehzad Z, Margulies DS, Kelly AM, Uddin LQ, Gotimer K, Biswal BB, Castellanos FX, Milham MP.** Functional connectivity of the human amygdala using resting state fMRI. *Neuroimage* 45: 614–626, 2009.
- Russchen FT, Bakst I, Amaral DG, Price JL.** The amygdalostriatal projections in the monkey. An anterograde tracing study. *Brain Res* 329: 241–257, 1985.
- Saint-Cyr JA, Ungerleider LG, Desimone R.** Organization of visual cortical inputs to the striatum and subsequent outputs to the pallido-nigral complex in the monkey. *J Comp Neurol* 298: 129–156, 1990.
- Ségonne F, Dale AM, Busa E, Glessner M, Salat D, Hahn HK, Fischl B.** A hybrid approach to the skull stripping problem in MRI. *Neuroimage* 22: 1060–1075, 2004.
- Ségonne F, Pacheco J, Fischl B.** Geometrically accurate topology-correction of cortical surfaces using nonseparating loops. *IEEE Trans Med Imaging* 26: 518–529, 2007.
- Selemon LD, Goldman-Rakic PS.** Longitudinal topography and interdigitation of corticostriatal projections in the rhesus monkey. *J Neurosci* 5: 776–794, 1985.
- Smith SM, Jenkinson M, Woolrich MW, Beckmann CF, Behrens TE, Johansen-Berg H, Bannister PR, De Luca M, Doherty J, Flitney D, Niazy RK, Saunders J, Vickers J, Zhang Y, De Stefano N, Brady JM, Matthews PM.** Advances in functional and structural MR image analysis and implementation as FSL. *Neuroimage* 23: S208–S219, 2004.
- Stanton GB, Goldberg ME, Bruce CJ.** Frontal eye field efferents in the macaque monkey. I. Subcortical pathways and topography of striatal and thalamic terminal fields. *J Comp Neurol* 271: 473–492, 1988.
- Strick PL, Dum RP, Mushiake H.** Basal ganglia “loops” with the cerebral cortex. In: *Functions of the Cortico-Basal Ganglia Loop*, edited by Graybiel AM, Kimura M. Tokyo: Springer, 1995.
- Takada M, Tokuno H, Hamada I, Inase M, Ito Y, Imanishi M, Hasegawa N, Akazawa T, Hatanaka N, Nambu A.** Organization of inputs from cingulate motor areas to basal ganglia in macaque monkey. *Eur J Neurosci* 14: 1633–1650, 2001.
- Takada M, Tokuno H, Nambu A, Inase M.** Corticostriatal input zones from the supplementary motor area overlap those from the contra- rather than ipsilateral primary motor cortex. *Brain Res* 791: 335–340, 1998a.
- Takada M, Tokuno H, Nambu A, Inase M.** Corticostriatal projections from the somatic motor areas of the frontal cortex in the macaque monkey: segregation versus overlap of input zones from the primary motor cortex, the supplementary motor area, and the premotor cortex. *Exp Brain Res* 120: 114–128, 1998b.
- Talairach J, Tournoux P.** *Co-planar Stereotaxic Atlas of the Human Brain: 3-Dimensional Proportional System: an Approach to Cerebral Imaging*. New York: Thieme, 1988.
- Ungerleider LG, Desimone R, Galkin TW, Mishkin M.** Subcortical projections of area MT in the macaque. *J Comp Neurol* 223: 368–386, 1984.
- van der Kouwe AJ, Benner T, Fischl B, Schmitt F, Salat DH, Harder M, Sorenson AG, Dale AM.** On-line automatic slice positioning for brain MR imaging. *Neuroimage* 27: 222–230, 2005.
- van der Kouwe AJ, Benner T, Salat DH, Fischl B.** Brain morphometry with multiecho MPRAGE. *Neuroimage* 40: 559–569, 2008.
- Van Dijk KR, Hedden T, Venkataraman A, Evans KC, Lazar SW, Buckner RL.** Intrinsic functional connectivity as a tool for human connectomics: theory, properties, and optimization. *J Neurophysiol* 103: 297–321, 2010.
- Van Dijk KR, Sabuncu MR, Buckner RL.** The influence of head motion on intrinsic functional connectivity MRI. *Neuroimage* 59: 431–438, 2012.
- Van Essen DC.** A Population-Average, Landmark-and Surface-based (PALS) atlas of human cerebral cortex. *Neuroimage* 28: 635–662, 2005.
- Van Essen DC, Dierker DL.** Surface-based and probabilistic atlases of primate cerebral cortex. *Neuron* 56: 209–225, 2007.
- Van Hoesen GW, Yeterian EH, Lavizzo-Mourey R.** Widespread corticostriate projections from temporal cortex of the rhesus monkey. *J Comp Neurol* 199: 205–219, 1981.
- Yeo BT, Krienen FM, Sepulcre J, Sabuncu MR, Lashkari D, Hollinshead M, Roffman JL, Smoller JW, Zollei L, Polimeni JR, Fischl B, Liu H, Buckner RL.** The organization of the human cerebral cortex estimated by intrinsic functional connectivity. *J Neurophysiol* 106: 1125–1165, 2011.
- Yeterian EH, Pandya DN.** Prefrontostriatal connections in relation to cortical architectonic organization in rhesus monkeys. *J Comp Neurol* 312: 43–67, 1991.
- Yeterian EH, Pandya DN.** Striatal connections of the parietal association cortices in rhesus monkeys. *J Comp Neurol* 332: 175–197, 1993.
- Yeterian EH, Pandya DN.** Corticostriatal connections of the superior temporal region in rhesus monkeys. *J Comp Neurol* 399: 384–402, 1998.
- Yeterian EH, Van Hoesen GW.** Cortico-striate projections in the rhesus monkey: the organization of certain cortico-caudate connections. *Brain Res* 139: 43–63, 1978.
- Zhang D, Snyder AZ, Fox MD, Sansbury MW, Shimony JS, Raichle ME.** Intrinsic functional relations between human cerebral cortex and thalamus. *J Neurophysiol* 100: 1740–1748, 2008.